ARCHIVIO ISTITUZIONALE
DELLA RICERCA

Alma Mater Studiorum Università di Bologna
Archivio istituzionale della ricerca

State augmentation method for multimode nonstationary vibrations of long-span bridges under extreme winds

This is the final peer-reviewed author's accepted manuscript (postprint) of the following publication:

Published Version:
Lei, S., Cui, W., Patruno, L., De Miranda, S., Zhao, L., Ge, Y. (2025). State augmentation method for multimode nonstationary vibrations of long-span bridges under extreme winds. ENGINEERING STRUCTURES, 332, 1-18 [10.1016/j.engstruct.2025.120021].

Availability:
This version is available at: https://hdl.handle.net/11585/1035517 since: 2026-01-07

Published:

DOI: http://doi.org/10.1016/j.engstruct.2025.120021

Terms of use:

Some rights reserved. The terms and conditions for the reuse of this version of the manuscript are specified in the publishing policy. For all terms of use and more information see the publisher's website.

This item was downloaded from IRIS Università di Bologna (https://cris.unibo.it/).
When citing, please refer to the published version.

(Article begins on next page)

15 October 2026

State augmentation method for multimode nonstationary vibrations of long-span bridges under extreme winds

Simian Lei[1, 2, 3, 4], Wei Cui[1, 2, 3, *], Luca Patruno[4], Stefano de Miranda[4], Lin Zhao[1, 2, 3], Yaojun Ge[1, 2, 3]

[1] State Key Lab of Disaster Reduction in Civil Engineering, Tongji University, Shanghai 200092, China

[2] Department of Bridge Engineering, College of Civil Engineering, Tongji University, Shanghai 200092, China

[3] Key Laboratory of Transport Industry of Bridge Wind Resistance Technologies, Tongji University, Shanghai 200092, China

[4] DICAM, University of Bologna, Bologna 40121, Italy

Abstract

Stochastic dynamic analysis frequently relies on the assumption of time independence of linear systems and the stationarity of stochastic excitations, facilitating a variety of engineering studies. Nevertheless, these assumptions may not consistently remain valid, particularly in cases of structural vibrations induced by nonstationary extreme winds, and can lead to inaccurate predictions. The excitations in these scenarios have notable nonstationary characteristics because of the unstable nature of the flow. In addition, when aeroelastic forces are considered, the combined aerodynamic-mechanical system transforms into a linear time-varying system with aerodynamic damping and stiffness that change over time. In this work, a state augmentation approach for computing the multimode vibrations of a long-span bridge under nonstationary wind conditions is presented. The methodology integrates both nonstationary turbulence-induced forces and unsteady motion-induced forces. The coupling between motion-induced forces and bridge vibrations renders the system damping and stiffness matrices both time-varying and asymmetric; this results in complex-valued modes and coupled dynamics that cannot be adequately captured by a single-degree-of-freedom (SDOF) model. The proposed multi-degree-of-freedom (MDOF) approach is a stochastic calculus-based method that avoids complex modal analysis. The statistical moments of all orders for the responses of the MDOF systems are derived via Itô's formula and the stars and bars approach. Compared with existing approaches, the new approach is both reliable and efficient, demonstrating its potential for accurate and efficient analysis of nonstationary vibrations in complex engineering systems.

Keywords

Nonstationary wind; Multimode buffeting; Moment equations; Linear time-varying system; Itô's formula.

1 Introduction

The stochastic analysis of dynamic systems has long been crucial in mechanical and structural engineering [1] and is driven by the growing need to assess structural reliability from a probabilistic perspective. Typically, both structures and excitations are believed to have unchanging features over time. Excitations are treated as stationary processes, and systems are regarded as linear time-invariant. These assumptions often provide adequate precision for a broad range of applications, including vehicle-track dynamic systems subjected to track irregularities [2] and civil structures exposed to synoptic winds [3, 4]. However, in certain scenarios, these assumptions may not hold true, leading to inaccuracies. For example, when a train passes a bridge, the

* Corresponding author, E-mail address: cuiwei@tongji.edu.cn (W. Cui).

This is the accepted manuscript version of the article.

The final published version of this article is available at https://doi.org/10.1016/j.engstruct.2025.120021

© 2025. Licensed under the CC-BY-NC-ND 4.0 license https://creativecommons.org/licenses/by-nc-nd/4.0/

coupled system exhibits time-dependent features [5], and extreme wind events such as typhoons and downbursts display significant nonstationary characteristics [6, 7], with time-varying means and nonstationary fluctuations. Unlike stationary processes, which have consistent physical meanings, nonstationary processes can be characterized in multiple ways, such as through wavelet spectra [8] and Hilbert spectra [9]. Nevertheless, these techniques often lack a clear explanation in terms of physical phenomena, especially in regard to the local distribution of energy across different frequencies. Consequently, the original signal using these spectra is difficult to accurately reconstruct. Priestley's evolutionary spectra provide a theoretical framework that explains the energy distribution of processes that are not steady across different frequencies and their evolution over time. The presence of time-dependent characteristics in systems and nonstationary excitations causes challenges for stochastic dynamic analysis.

The focus of this study is on structural vibrations induced by nonstationary winds, which have gained considerable attention in recent years [6, 7]. Nonstationary flows can cause rapid fluctuations that have the potential to increase aerodynamic forces, resulting in greater structural responses [10]. Traditional buffeting analysis typically relies on modal superposition methods, which often disregard the aerodynamic coupling effects among modes. Importantly, slender structures, such as long-span bridges, inherently possess modes that are closely spaced. [11]. As bridge spans increase, concerns arise regarding the influence of aerodynamic damping and stiffness on structural dynamics and the potential for coupling effects in multimode buffeting vibrations [12]. This highlights the necessity of incorporating motion-induced forces for accurate predictions of buffeting responses; this topic has received increasing attention in recent decades [13]. When aeroelastic effects are considered [14], the coupled aerodynamic-mechanical system is defined as a linear time-varying (LTV) system [15] since the aerodynamic stiffness and damping vary with time because of the changing kinetic pressure. Notably, the system response for LTV systems is not stationary [16], even in the case of stationary excitations. Brusco and Solari [14] accounted for aeroelastic forces and calculated the vibrations of thin structures exposed to nonstationary thunderstorm flows by integrating the equation of motion in the time domain. Nonetheless, the literature on these effects remains limited since classical methodologies are designed primarily for synoptic winds [17]. Consequently, statistically evaluating nonstationary responses is challenging, particularly when unsteady effects are considered [3, 4].

To statistically characterize nonstationary responses, Monte Carlo simulations [18] can generate numerous time-history samples from the evolutionary spectrum [19, 20]. Nevertheless, these simulations quickly become computationally demanding when a large number of samples are needed to obtain reliable results [1, 21]. Kareem et al. [17], building on Priestley's evolutionary spectra theory [19, 20] and the seminal work of Davenport [3, 4], expanded the widely accepted wind loading chain from analysis in the stationary frequency domain to the nonstationary regime in the time-frequency domain. In the generalized wind loading chain, the response spectrum is determined by multiplying the evolutionary wind spectra, the instantaneous aerodynamic admittance, and the fixed mechanical admittance [22]. This approach has since been applied [23] to predict nonstationary buffeting responses in the presence of aerodynamic forces with time-varying coefficients. To handle systems with time-varying features, this approach considers the system to be fixed within each small sliding time window [24, 25], reducing the problem to determining the fixed admittance function and the stationary responses in each window. Thus, this method is more suitable for systems with

gradually changing features. An alternative time-frequency approach, the pseudo excitation method proposed by Lin et al. [26], is capable of considering both time-varying characteristics and nonstationary excitations simultaneously [25, 27]. This is achieved by expanding the pseudo excitation in the frequency domain and then integrating the corresponding response in the time domain. Concerns arise with these time-frequency approaches if the response spectrum is not of interest, but only its statistical moments are needed. As noted in [28], the total computing time is consumed mainly when the spectrum is integrated and is approximately proportional to the number of frequencies. The precise integration method [29] can be employed to improve computing efficiency, but it still requires calculations in the frequency domain.

In parallel with the abovementioned contributions, Grigoriu [30-32] proposed a seminal work utilizing stochastic calculus [33, 34] to study linear systems with stationary non-Gaussian inputs expressed as polynomial functions of Gaussian processes. The core idea is that the excitations can be approximated by filtered Brownian motions [1], allowing dynamic equations to be transformed into stochastic differential equations. By using Itô's formula [34], the response moments can be immediately computed by solving the so-called moment equations, achieving high efficiency and avoiding the need for frequency domain analysis. This method is closely related to the Fokker-Planck (FPK) equation [35]. The moment equations can be equivalently derived by applying the Mellin transform to the FPK equation [36, 37], converting the partial differential equation describing the probability density function into an algebraic equation in terms of statistical moments. The potential of this method has been extensively examined by several researchers for both non-Gaussian excitations [1, 38, 39] and nonlinear systems with nonlinear and parametric excitations [40, 41]. When dealing with non-Gaussian scenarios, the moment equations are derived as a closed set of algebraic equations. This allows for the calculation of high-order moments to characterize the non-Gaussian behavior of the responses. Revisiting this concept, Cui et al. [42] considered the multimodal coupling effect and calculated the response moments of long-span bridges under non-Gaussian wind turbulence. In the case of nonlinear systems, nonlinearity renders the system unclosed; thus, moments of the current order depend on moments of higher orders that have not yet been determined. To address this, additional closure tactics [43] need to be introduced to make the problem solvable.

As discussed, even though the method has been established for decades, its application has focused predominantly on theoretical aspects, such as closure methods, fractional Brownian motion [44], and fractional moments [37], with limited practical applications reported for analyzing nonstationary vibrations, especially for time-varying systems. This presents significant practical challenges. A recent work by Lei et al. [45] demonstrated the potential of this method for nonstationary buffeting analysis considering aeroelastic forces. The methodology involved significant changes, such as transforming algebraic moment equations in a stationary case into differential equations in a nonstationary case. However, that application was limited to a system with only one degree of freedom (DOF) and employs quasi-steady theory [14] in modeling aerodynamic forces. As shown by Cui [42], applying this method to multi-DOF systems and considering higher-order moments have significantly complicated the process; thus, manual derivation of the moment equations is virtually impossible.

Moreover, as the aeroelastic effect becomes increasingly pronounced in bridge dynamics with increasing bridge span [11, 46, 47], accurate modeling of turbulence-induced and motion-induced forces, including

unsteady effects, becomes essential. The modeling of the aerodynamic forces on bluff bodies has been conducted predominantly in the frequency domain [48] to capture their frequency-dependent nature, commonly referred to as the unsteady aerodynamic effect. Inspired by seminal studies on thin airfoils [49], Scanlan introduced flutter derivatives [48], which relied on experimental quantification to characterize unsteady motion-induced forces on bridge decks with harmonic motions. However, for bridge decks subjected to arbitrary motions and turbulence, the use of convolution techniques to calculate aerodynamic forces in the time domain was impractical because of difficulties in transforming these frequency-dependent aerodynamic parameters into impulse response functions. To address this challenge, Chen and Kareem [50] approximated aerodynamic transfer functions in a rational function format, enabling an easy inverse Fourier transform to derive unsteady aerodynamic forces in the time domain using a set of linear differential equations. Additionally, Diana et al. [51-53] proposed rheological models that use mechanical elements such as springs, dampers and masses to reproduce both motion-induced and turbulence-induced forces in the time domain. By introducing additional DOFs, these models provide effective solutions for considering fluid-structure interactions in time-domain analyses. Note that these problems become more difficult when non-Gaussian and nonstationary conditions are included. the challenges posed by multi-DOF systems and unsteady aerodynamic effects need to be solved to expand the practicability of the moment equation approach.

The objective of this study is to propose a state augmentation method for calculating the multimode vibrations in long-span bridges subjected to nonstationary wind. The nonstationary wind speed is modeled as the superposition of a time-varying mean and a uniformly modulated process using Priestley's evolutionary theory. The model incorporates both the unsteady aerodynamic forces induced by structural motions and nonstationary turbulence. The dynamic equations of the coupled wind-bridge system include the effects of time-varying aerodynamic damping and stiffness and are described as a linear time-varying system. By applying Itô's Formula, the stochastic vibration problem is transformed into a deterministic problem, and the statistical response moments are obtained by solving a set of first-order differential equations. This approach directly addresses time-dependent and nonstationary characteristics without relying on spectral or frequency-domain analysis, distinguishing it from existing methods such as the pseudo excitation method or the evolutionary wind loading chain. The proposed approach is first verified in a stationary case by comparing the results with those obtained using the well-established frequency-domain approach. This method is subsequently applied to compute nonstationary responses to realistic nonstationary wind conditions, and a specific procedure is introduced to preprocess the wind data. The benefits of the proposed approach and the nonstationary characteristics of the responses are discussed in detail. This study is regarded as an extension of the study by Lei et al. [45], generalizing the previous study of an SDOF case to an MDOF model including unsteady aerodynamic forces.

2 Formulation of the state augmentation method

This section first establishes the proposed methodology from a theoretical perspective, ensuring its generality and applicability across various engineering problems. The application of this methodology to the specific case of bridge buffeting is demonstrated in the following section.

2.1 Statement of the problem

A linear time-varying (LTV) system with N DOFs under nonstationary Gaussian excitations is

considered. The dynamic equations of the system are represented by a set of linear differential equations with coefficients that change with time:

$$\mathbf{M}\ddot{\mathbf{X}} + \mathbf{C}(t)\dot{\mathbf{X}} + \mathbf{K}(t)\mathbf{X} = \mathbf{F}(t) \tag{1}$$

where $\mathbf{M}$ is the mass matrix, $\mathbf{C}(t)$ is the time-varying damping matrix, $\mathbf{K}(t)$ is the time-varying stiffness matrix, $\mathbf{F}(t)$ is the nonstationary excitation vector, and $\mathbf{X}$ is the displacement response vector.

Nonstationary processes can be defined in multiple ways [9, 54, 55], in contrast to stationary processes, which have a definite definition of the power spectrum. The focus of this work is exclusively on the evolutionary process proposed by Priestley [19, 20]. This nonstationary process can be considered the output of a linear filter through which stationary processes pass, and it provides a meaningful representation of the local distribution of energy over frequencies and its evolution over time. In this study for simplicity, the nonstationary excitation $\mathbf{F}(t)$ is represented by a uniformly time-modulated model [6], which applies to the majority of real-world engineering problems [18]:

$$\mathbf{F}(t) = \mathbf{A}(t)\mathbf{F}_s(t) \tag{2}$$

where $\mathbf{A}(t)$ is the modulation function and $\mathbf{F}_s(t)$ is the derived stationary process.

The dynamic equation is converted to its state-space form by substituting Eq. (2) into Eq. (1):

$$\frac{\mathrm{d}}{\mathrm{d}t}\begin{bmatrix}\mathbf{X}\\ \dot{\mathbf{X}}\end{bmatrix} = \begin{bmatrix}\mathbf{0} & \mathbf{I}\\ -\mathbf{M}^{-1}\mathbf{K}(t) & -\mathbf{M}^{-1}\mathbf{C}(t)\end{bmatrix}\begin{bmatrix}\mathbf{X}\\ \dot{\mathbf{X}}\end{bmatrix} + \begin{bmatrix}\mathbf{0}\\ \mathbf{M}^{-1}\mathbf{A}(t)\mathbf{F}_s\end{bmatrix} \tag{3}$$

2.2 Augmented states of the system and the excitation

According to [30, 32], a multivariate Ornstein-Uhlenbeck (OU) process $\mathbf{Z}(t)$ can be used to approximate the stationary process $\mathbf{F}_s(t)$ and follows a stochastic differential equation:

$$\mathrm{d}\mathbf{Z}(t) = -\boldsymbol{\alpha}\mathbf{Z}(t)\mathrm{d}t + \boldsymbol{\Theta}\mathrm{d}\mathbf{W}(t) \tag{4}$$

where $\boldsymbol{\alpha}$ and $\boldsymbol{\Theta}$ are time-independent positive definite coefficient matrices; and $\mathbf{W}(t)$ is a multivariate Wiener process with components that are mutually independent and satisfies $\mathrm{E}[\mathrm{d}\mathbf{W}\cdot\mathrm{d}\mathbf{W}^{\mathrm{T}}] = \mathbf{I}_M\mathrm{d}t$, with $\mathbf{I}_M$ being the identity matrix and $\mathrm{E}[\cdot]$ being the expectation operator. The Wiener process is commonly used to represent Brownian motion, and its derivative is the white noise Gaussian process. Note that the dimensions of $\mathbf{Z}(t)$ and $\mathbf{W}(t)$ are denoted as M here to account for situations where the size of OU processes can be different from the system dimensions, and this aspect will be considered in Section 3.5. Eq. (4) essentially acts as a linear filter that transforms the white noise signal associated with $\mathbf{W}(t)$ into colored noise, i.e., OU processes. This transformation allows the OU processes to approximate the system excitations. $\boldsymbol{\alpha}$ and $\boldsymbol{\Theta}$ can be obtained by fitting the PSD matrix of the OU process, $\mathbf{S}_{\mathbf{ZZ}}(\mathrm{j}\omega) = (-\mathrm{j}\omega\mathbf{I}_M + \boldsymbol{\alpha})^{-1}\boldsymbol{\Theta}\boldsymbol{\Theta}^{\mathrm{T}}(\mathrm{j}\omega\mathbf{I}_M + \boldsymbol{\alpha}^{\mathrm{T}})^{-1}$, with that of $\mathbf{F}_s(t)$. The autocovariance matrix $\mathbf{K}_{\mathbf{ZZ}}$ can be calculated using the Lyapunov equation [56]:

$$\boldsymbol{\alpha}\mathbf{K}_{\mathbf{ZZ}} + \mathbf{K}_{\mathbf{ZZ}}\boldsymbol{\alpha}^{\mathrm{T}} = \boldsymbol{\Theta}\boldsymbol{\Theta}^{\mathrm{T}} \tag{5}$$

The fitting procedure for the OU process is detailed in Section 4.

Since the OU process is characterized by a first-order differential equation and corresponds to a ω^{-2} order in its PSD, a slight mismatch with the wind load always occurs since the wind spectrum typically has a slope of approximately -5/3 at high frequencies. This may lead to inaccuracies in predicting the nonstationary buffeting response in the high-frequency range, particularly when higher-order modes of structures are considered. To address this fundamental issue, incorporating fractional derivatives may be beneficial, although the implementation would require complex mathematics and could substantially alter the proposed

methodology, such as involving fractional-order moments. Nevertheless, this technique enhances the precision of buffeting prediction, especially as the number of DOFs increases. The incorporation of fractional derivatives is being considered in ongoing research.

By substituting Eq. (4) into Eq. (3), the system states and excitations can be represented as the following augmented equation:

$$\mathrm{d}\begin{bmatrix}\mathbf{X}\\ \dot{\mathbf{X}}\\ \mathbf{Z}\end{bmatrix}=\begin{bmatrix}\mathbf{0} & \mathbf{I} & \mathbf{0}\\ -\mathbf{M}^{-1}\mathbf{K}(t) & -\mathbf{M}^{-1}\mathbf{C}(t) & \mathbf{M}^{-1}\mathbf{A}(t)\\ \mathbf{0} & \mathbf{0} & -\boldsymbol{\alpha}\end{bmatrix}\begin{bmatrix}\mathbf{X}\\ \dot{\mathbf{X}}\\ \mathbf{Z}\end{bmatrix}\mathrm{d}t+\begin{bmatrix}\mathbf{0}\\ \mathbf{0}\\ \boldsymbol{\Theta}\end{bmatrix}\mathrm{d}\mathbf{W} \tag{6}$$

Eq. (6) is considered a stochastic differential equation [33] of the Itô-type form:

$$\mathrm{d}\mathbf{Y}(t)=\mathbf{g}(\mathbf{Y}(t),t)\mathrm{d}t+\mathbf{h}(\mathbf{Y}(t),t)\mathrm{d}\mathbf{W} \tag{7}$$

where $\mathbf{Y}(t)$ is an $2N+M$-dimensional vector of augmented states, and $\mathbf{g}(\mathbf{Y}(t),t)$ and $\mathbf{h}(\mathbf{Y}(t),t)$ are functions of $\mathbf{Y}(t)$ and t. By introducing OU processes, the buffeting equation is converted into a stochastic differential equation, enabling the application of relevant stochastic calculus theories.

2.3 Differential equations satisfied by statistical moments

$\xi(\mathbf{Y}(t),t)$ is assumed to be a scalar-valued function of the augmented states $\mathbf{Y}(t)$ and time t, for instance, the moments function of$\mathbf{Y}(t)$ is defined as follows:

$$\xi(\mathbf{Y})=\prod_{i}^{N}X_i^{a_i}\prod_{i}^{N}\dot{X}_i^{b_i}\prod_{i}^{M}Z_i^{f_i} \tag{8}$$

where X_i, $\dot{X}_i$ and Z_i represent the i-th element of the states $\mathbf{X}$, $\dot{\mathbf{X}}$ and $\mathbf{Z}$, respectively. The exponents a_i, b_i and f_i are the corresponding nonnegative integer exponents.

According to Itô's formula [34], the total derivative of $\xi(\mathbf{Y}(t),t)$ is expanded in the form of a stochastic differential equation:

$$\mathrm{d}\xi=\left\{\frac{\partial\xi}{\partial t}+[\nabla_{\mathbf{Y}}(\xi)]^{\mathrm{T}}\mathbf{g}+\frac{1}{2}\mathrm{Tr}(\mathbf{h}^{\mathrm{T}}[\mathrm{H}_{\mathbf{Y}}(\xi)]\mathbf{h})\right\}\mathrm{d}t+[\nabla_{\mathbf{Y}}(\xi)]^{\mathrm{T}}\mathbf{h}\mathrm{d}\mathbf{W} \tag{9}$$

where $\mathrm{H}_{\mathbf{Y}}(\xi)$ and $\nabla_{\mathbf{Y}}(\xi)$ denote the Hessian matrix and the gradient vector of ξ with respect to $\mathbf{Y}$, respectively. The superscript T is the transpose operator, and $\mathrm{Tr}(\cdot)$ denotes the trace of a matrix.

Since the expectation of $\mathrm{d}\mathbf{W}$ is zero, by evaluating the expectation of Eq. (9) [30], an intricate stochastic differential equation is reduced to the following solvable deterministic differential equation:

$$\frac{\mathrm{d}}{\mathrm{d}t}\mathrm{E}[\xi]=\mathrm{E}\left[\frac{\partial\xi}{\partial t}\right]+\sum_{i}^{2N+M}\mathrm{E}\left[\frac{\partial\xi}{\partial Y_i}g_i\right]+\frac{1}{2}\sum_{i}^{2N+M}\sum_{j}^{2N+M}\mathrm{E}\left[(\mathbf{h}\mathbf{h}^{\mathrm{T}})_{ij}\frac{\partial^2\xi}{\partial Y_j\partial Y_i}\right] \tag{10}$$

where Y_i is the i-th element of $\mathbf{Y}(t)$, and g_i is the i-th element of $\mathbf{g}(\mathbf{Y}(t),t)$. In particular, $\mathrm{E}[\partial\xi/\partial t]$ is zero if there is no explicit time dependence in ξ, e.g., Eq. (8), and $\mathrm{d}\mathrm{E}[\xi]/\mathrm{d}t$ is not constant zero in the case of nonstationary $\mathbf{Y}$ [30].

By considering $\mathrm{E}[\partial\xi/\partial t]=0$ and substituting Eq. (8) into Eq. (10), Eq. (10) expands to the following:

$$\frac{\mathrm{d}}{\mathrm{d}t}\mathrm{E}\left[\prod_i^N X_i^{a_i}\prod_i^N \dot{X}_i^{b_i}\prod_i^M Z_i^{f_i}\right]=\sum_{r=1}^N a_r\mathrm{E}\left[X_r^{-1}g_r\prod_i^N X_i^{a_i}\prod_i^N \dot{X}_i^{b_i}\prod_i^M Z_i^{f_i}\right]$$
$$+\sum_{r=1}^N b_r\mathrm{E}\left[\dot{X}_r^{-1}g_{r+N}\prod_i^N X_i^{a_i}\prod_i^N \dot{X}_i^{b_i}\prod_i^M Z_i^{f_i}\right]+\sum_{r=1}^M f_r\mathrm{E}\left[Z_r^{-1}g_{r+2N}\prod_i^N X_i^{a_i}\prod_i^N \dot{X}_i^{b_i}\prod_i^M Z_i^{f_i}\right]$$
$$+\frac{1}{2}\sum_{\substack{r=1\\r\neq s}}^M\sum_{s=1}^M(\boldsymbol{\Theta}\boldsymbol{\Theta}^{\mathrm{T}})_{rs}f_rf_s\mathrm{E}\left[Z_r^{-1}Z_s^{-1}\prod_i^N X_i^{a_i}\prod_i^N \dot{X}_i^{b_i}\prod_i^M Z_i^{f_i}\right]$$
$$+\frac{1}{2}\sum_{r=1}^M(\boldsymbol{\Theta}\boldsymbol{\Theta}^{\mathrm{T}})_{rr}f_r(f_r-1)\mathrm{E}\left[Z_r^{-2}\prod_i^N X_i^{a_i}\prod_i^N \dot{X}_i^{b_i}\prod_i^M Z_i^{f_i}\right] \tag{11}$$

Moreover, the expected value of the moments function on each side of Eq. (11) is exactly the statistical moment of $\mathbf{Y}$. For brevity, the statistical moment $\mathrm{E}\left[\prod_i^N X_i^{a_i}\prod_i^N \dot{X}_i^{b_i}\prod_i^M Z_i^{f_i}\right]$ is denoted as $\mathrm{m}(a_1,\cdots,a_N,b_1,\cdots,b_N,f_1,\cdots,f_M)$ and the summation of the exponents $s=\sum_{i=1}^N(a_i+b_i)+\sum_{i=1}^M f_i$, is the moment order. The left-hand side of Eq. (11) is represented by $\dot{\mathrm{m}}(a_1,\cdots,a_N,b_1,\cdots,b_N,f_1,\cdots,f_M)$, which represents the first derivative of the moment of order s. On the right-hand side of Eq. (11), the first three summations come from the gradient term of Eq. (10) and consist of the function $\mathbf{g}$ and the first-order derivative. Since $\mathbf{g}$ is a linear function of the states $\mathbf{X}$, $\dot{\mathbf{X}}$ and $\mathbf{Z}$, the moments in the first three summations have the same order of s but with different combinations of exponents. The two remaining terms on the RHS of Eq. (11) come from the Hessian matrix term of Eq. (10) and consist of the constant Hessian matrix $\mathbf{h}$ and second-order derivatives. Consequently, the corresponding moments have the order of $s-2$. In particular, the moments in Eq. (11) will be zero when any exponent is negative, and $\mathrm{m}(0,\cdots,0,0,\cdots,0,f_1,\cdots,f_M)$ are the known statistical moments of OU excitations when $a_i=b_i=0$.

By substituting all possible combinations of exponents with a given order of s, Eq. (11) can be reorganized as follows:

$$\dot{\mathbf{m}}_s=\mathbf{P}_1(t)\mathbf{m}_s+\mathbf{Q}_1(t)+\mathbf{P}_2\mathbf{m}_{s-2}+\mathbf{Q}_2 \tag{12}$$

where $\mathbf{m}_s$ and $\mathbf{m}_{s-2}$ represent vectors containing all unknown statistical moments of order s and $s-2$, respectively. $\mathbf{P}_1$, $\mathbf{P}_2$, $\mathbf{Q}_1$ and $\mathbf{Q}_2$ are the coefficient matrices associated with system properties and the statistical moments of OU processes.

These formulas constitute the state augmentation method (SAM). The statistical moments are described by a set of first-order differential equations, i.e., Eq. (12). Given initial values, the moments of each order s can be determined immediately by solving Eq. (12) without undergoing an intermediate stage, such as the response spectrum. Importantly, the response moments of higher order are dependent on lower-order moments, as described by Eq. (12). Specifically, moments of order s depend on moments of order $s-2$, necessitating solving the moment equations in a recursive manner, closed by imposing the boundary condition $\mathbf{m}_0=\mathbf{1}$. However, an exception exists: second-order moments ($s=2$) depend on zero-order moments ($s=0$), which are the known moments of Ornstein-Uhlenbeck (OU) excitations. This allows second-order moments to be directly obtained by solving the moment equations without recursion. Since only the second-order moments are of interest in this research, the moment equations can be directly solved. However, solving the equations for higher-order moments, such as skewness ($s=3$) and kurtosis ($s=4$) in non-Gaussian problems, requires

first obtaining moments of lower order, such as the mean ($s = 1$) and variance ($s = 2$), involving a recursive process.

2.4 Combinations of the exponents

Once the statistical moment equations, i.e., Eq. (12), have been derived, the statistical moments of the nonstationary responses of systems with any number of degrees of freedom (DOFs) can be easily evaluated. However, as the number of DOFs increases, manually deriving the moment equations becomes impractical due to the complexity involved, especially for linear time-varying (LTV) systems with many DOFs.

To address this challenge, a strategy for assembling the differential equations (Eq. (12)) is needed. In essence, the issue boils down to determining all possible combinations of the moments and the total number of these combinations. This translates to solving a single linear equation that contains multiple variables, as follows:

$$a_1 + \cdots + a_N + b_1 + \cdots + b_N + f_1 + \cdots + f_M = s \tag{13}$$

under the condition of all nonnegative integer variables, i.e., $a_i \geq 0$, $b_i \geq 0$ and $f_i \geq 0$. This can be equivalently converted into the following equation:

$$a_1' + \cdots + a_N' + b_1' + \cdots + b_N' + f_1' + \cdots + f_M' = s + 2N + M \tag{14}$$

where the variables are converted as follows: $a_i' = a_i + 1 \geq 1$, $b_i' = b_i + 1 \geq 1$ and $f_i' = f_i + 1 \geq 1$.

The stars and bars approach [57] from combinatorics can be employed to solve this problem. The technique helps determine how to distribute a given number of indistinguishable items (stars) into distinct groups (bins) with no empty groups. For example, if there are $s + 2N + M$ stars to be allocated across $2N + M$ bins, the problem can be visualized by inserting $2N + M - 1$ bars between the stars, ensuring that no bin is empty, as illustrated in Figure 1.

★★★★|★|★★|★★★★★|★

Fig. 1. $2N + M - 1$ bars producing $2N + M$ bins containing a total of $s + 2N + M$ stars.

By combining this combinatorial method with symbolic calculations [58], the moment equations for dynamic systems can be automatically constructed with any number of DOFs and for response moments of any order.

3 Nonstationary buffeting of long-span bridges

In this section, the nonstationary vibrations of long-span bridges under nonstationary winds are investigated using the state augmentation method developed in Section 2. The multimode dynamics of the bridge are considered to demonstrate the ability of the proposed approach to analyze nonstationary vibrations in multi-DOF structures.

3.1 Dynamics of bridge deck motions

Long-span bridges always have modal frequencies that are closely spaced [11]. In these flexible structures, significant coupling effects in multimode vibrations can arise because of the asymmetric aerodynamic damping and stiffness matrices when motion-induced forces are considered in buffeting analysis. Therefore, in this study, both nonstationary buffeting forces and motion-induced forces are included to predict the buffeting responses of the bridge.

The dynamic equation governing the motions of the bridge deck excited by nonstationary buffeting forces and motion-induced forces is as follows:

$$\mathbf{M}_d\ddot{\mathbf{X}}_d + \mathbf{C}_d\dot{\mathbf{X}}_d + \mathbf{K}_d\mathbf{X}_d = \mathbf{F}^{se} + \mathbf{F}^{b} \tag{15}$$

where $\mathbf{M}_d$, $\mathbf{C}_d$ and $\mathbf{K}_d$ are the mass, damping and stiffness matrices of the deck, respectively. The displacement vector $\mathbf{X}_d$ represents the motion in three directions at each node $\mathbf{X}_{di} = [p_i \quad h_i \quad \alpha_i]^{\mathrm{T}}$ $(i = 1, \cdots, N)$: sway p_i, hover h_i and pitch α_i, where N is the total number of nodes. The vectors $\mathbf{F}^b$ and $\mathbf{F}^{se}$ represent nonstationary buffeting forces and motion-induced forces, respectively, consisting of nodal forces in three directions: drag forces D^b and D^{se}, lift forces L^b and L^{se}, and pitching torques M^b and M^{se}. The motions of the deck induced by nonstationary aerodynamic forces are shown in Figure 2.

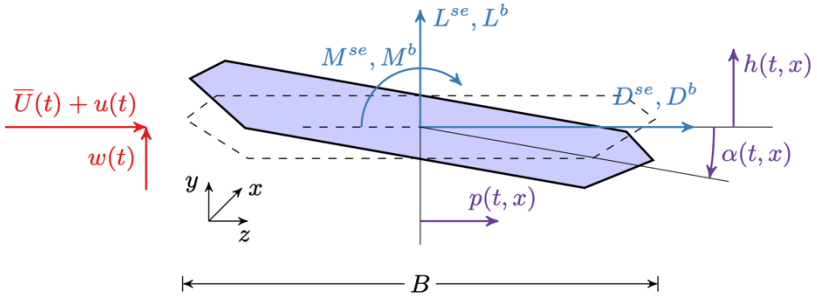

Fig. 2. Motions of the deck induced by the nonstationary aerodynamic forces.

3.2 Unsteady motion-induced forces in the time domain

The motion-induced forces for the deck with harmonic motions can be derived using Scanlan's flutter derivatives [48], which yields the following frequency-domain form:

$$\begin{bmatrix} \bar{D}_i^{se} \\ \bar{L}_i^{se} \\ \bar{M}_i^{se} \end{bmatrix} = \frac{1}{2}\rho U^2 \Delta L \begin{bmatrix} K^2(P_4^* + \mathrm{j}P_1^*) & K^2(P_6^* + \mathrm{j}P_5^*) & K^2(P_3^* + \mathrm{j}P_2^*)B \\ K^2(H_6^* + \mathrm{j}H_5^*) & K^2(H_4^* + \mathrm{j}H_1^*) & K^2(H_3^* + \mathrm{j}H_2^*)B \\ K^2(A_6^* + \mathrm{j}A_5^*)B & K^2(A_4^* + \mathrm{j}A_1^*)B & K^2(A_3^* + \mathrm{j}A_2^*)B^2 \end{bmatrix} \begin{bmatrix} \bar{p}_i \\ \bar{h}_i \\ \bar{\alpha}_i \end{bmatrix} \tag{16}$$

where $\bar{D}_i^{se}$, $\bar{L}_i^{se}$ and $\bar{M}_i^{se}$ are the frequency-dependent complex-valued amplitudes of the i-th nodal forces $\mathbf{F}_i^{se}$, and j is the imaginary unit; $\bar{h}_i$, $\bar{p}_i$ and $\bar{\alpha}_i$ are the amplitudes of motion; ΔL is the element length; B is the width of the deck; U represents the mean wind speed; $\rho = 1.25\ \mathrm{kg/m^3}$ and represents the air density; $K = \omega B/U$ and is the reduced frequency, where ω is the circular frequency; and H_i^*, P_i^* and A_i^* $(i = 1, 2, \cdots, 6)$ are flutter derivatives that are dependent on the reduced frequencies and geometric configurations of the deck. Given the relatively small magnitudes of the wind fluctuations and system responses compared with the mean wind speed, the variation in the effective wind attack angle is neglected, and the motion-induced forces are linearized around the mean static position.

The flutter derivatives are experimentally quantified only at discrete values. To facilitate the inverse transformation of motion-induced forces to the time domain, Roger's approximation technique [59] is employed to fit the flutter derivatives to rational functions:

$$\begin{bmatrix} K^2(P_4^* + \mathrm{j}P_1^*) & K^2(P_6^* + \mathrm{j}P_5^*) & K^2(P_3^* + \mathrm{j}P_2^*)B \\ K^2(H_6^* + \mathrm{j}H_5^*) & K^2(H_4^* + \mathrm{j}H_1^*) & K^2(H_3^* + \mathrm{j}H_2^*)B \\ K^2(A_6^* + \mathrm{j}A_5^*)B & K^2(A_4^* + \mathrm{j}A_1^*)B & K^2(A_3^* + \mathrm{j}A_2^*)B^2 \end{bmatrix} = \mathbf{A}_{i,1}^{se} + \mathrm{j}K\mathbf{A}_{i,2}^{se} + (\mathrm{j}K)^2\mathbf{A}_{i,3}^{se} + \sum_{l=1}^{m_{se}} \frac{\mathrm{j}K\mathbf{A}_{i,l+3}^{se}}{\mathrm{j}K + d_l^{se}} \tag{17}$$

where $\mathbf{A}_{i,1}^{se}$, $\mathbf{A}_{i,2}^{se}$, $\mathbf{A}_{i,3}^{se}$, $\mathbf{A}_{i,l+3}^{se}$, and $d_l^{se} \geq 0$ are frequency-independent coefficients and can be calibrated by fitting the data using the nonlinear least squares approach. The first three terms represent the aerodynamic stiffness, damping and mass, respectively. The unsteady aerodynamic effect is considered in rational terms,

where m_{se} represents the level of approximation accuracy. Note that in this study, the only source of the system's time-varying characteristic is the variation in the mean wind speed, which leads to time-varying kinetic pressure and, consequently, time-varying stiffness and damping matrices. Since the changes in the mean wind speeds are substantially slower than those of the structural responses, the inverse Fourier transformation of the force-motions can be performed as if the transfer matrix is fixed at each time instant.

The time-domain motion-induced forces can then be derived using an inverse Fourier transform method:

$$\mathbf{F}_i^{se} = \frac{1}{2}\rho U^2 \Delta L \left(\mathbf{A}_{i,1}^{se}\mathbf{X}_{di} + \frac{B}{U}\mathbf{A}_{i,2}^{se}\dot{\mathbf{X}}_{di} + \frac{B^2}{U^2}\mathbf{A}_{i,3}^{se}\ddot{\mathbf{X}}_{di} + \sum_{l=1}^{m_{se}} \boldsymbol{\phi}_{i,l}^{se} \right) \tag{18a}$$

The variables $\boldsymbol{\phi}_{i,l}^{se}$ are introduced to account for the unsteady effect and satisfy the following equation:

$$\dot{\boldsymbol{\phi}}_{i,l}^{se} = -\frac{d_l^{se} U}{B}\boldsymbol{\phi}_{i,l}^{se} + \mathbf{A}_{i,l+3}^{se}\dot{\mathbf{X}}_{di} \tag{18b}$$

The unsteady self-excited forces in Eq. (15) can thus be expressed as follows:

$$\mathbf{F}^{se} = \frac{1}{2}\rho U^2 \Delta L \left(\mathbf{A}_1^{se}\mathbf{X}_d + \frac{B}{U}\mathbf{A}_2^{se}\dot{\mathbf{X}}_d + \frac{B^2}{U^2}\mathbf{A}_3^{se}\ddot{\mathbf{X}}_d + \sum_{l=1}^{m_{se}} \boldsymbol{\phi}_l^{se} \right) \tag{19a}$$

in which the following is defined:

$$\dot{\boldsymbol{\phi}}_l^{se} = -\frac{d_l^{se} U}{B}\boldsymbol{\phi}_l^{se} + \mathbf{A}_{l+3}^{se}\dot{\mathbf{X}}_d \tag{19b}$$

where $\mathbf{A}_l^{se}$ is the partitioned diagonal matrix of $\mathbf{A}_{i,l}^{se}$ $(i = 1, \cdots, N)$.

The bridge tower has decoupled aerodynamics in the longitudinal and transverse directions due to its symmetric configuration and enable an SDOF model, as in previous research [45]; however, the vertical and rotational aerodynamics of bridge beams are inherently coupled due to their asymmetric configuration, as indicated in Eq. (16). This coupling leads to a typical MDOF dynamics problem (further discussions are provided in Section 3.5).

3.3 Nonstationary buffeting forces

As suggested in [6], the frequency content of nonstationary wind changes relatively slowly over time. In this study, nonstationary wind fluctuations are represented by the uniformly time-modulated model:

$$u(t) = \beta_u(t)u^s(t) \tag{20a}$$

$$w(t) = \beta_w(t)w^s(t) \tag{20b}$$

where the time-modulation functions $\beta_u(t)$ and $\beta_w(t)$ are slowly varying. $u^s(t)$ and $w^s(t)$ are derived zero-mean stationary Gaussian processes. Considering the large cyclone radius to bridge scale and virtually constant topographic features above the sea, the wind field around the bridge site is assumed to be horizontally homogeneous. Therefore, $\bar{U}(t)$, $\beta_u(t)$ and $\beta_w(t)$, the turbulence intensity, and the wind spectra are assumed to be uniformly distributed across the bridge. The partial coherence condition is considered for $u^s(t)$ and $w^s(t)$ at different nodes by using the exponentially decaying law for their coherence functions, as will be later detailed in Section 3.4. Note that $u(t)$ and $w(t)$ degrade into stationary wind fluctuations when $\beta_u(t)$ and $\beta_w(t)$ are constants. By using this model, the unsteady buffeting forces $\mathbf{F}_i^b$ can be rewritten as follows:

$$\mathbf{F}_i^b = \beta^u(t)\mathbf{F}_i^{bu} + \beta^w(t)\mathbf{F}_i^{bw} \tag{21}$$

where $\mathbf{F}_i^{bu}$ and $\mathbf{F}_i^{bw}$ are the unsteady buffeting forces contributed by $u_i^s(t)$ and $w_i^s(t)$ at the i-th node, respectively. Analogous to motion-induced forces, for stationary wind fluctuations with complex sinusoidal oscillations, $\mathbf{F}_i^{bu}$ and $\mathbf{F}_i^{bw}$ are given by the following:

$$\mathbf{F}_i^{bu} = \frac{1}{2}\rho U \Delta L \begin{bmatrix} 2BC_D\chi_{D_u} \\ 2BC_L\chi_{L_u} \\ 2B^2C_M\chi_{M_u} \end{bmatrix} u_i^s(t) = \frac{1}{2}\rho U \Delta L \boldsymbol{\chi}_i^u u_i^s \tag{22a}$$

$$\mathbf{F}_i^{bw} = \frac{1}{2}\rho U \Delta L \begin{bmatrix} B(C_D' - C_L)\chi_{D_w} \\ B(C_L' + C_D)\chi_{L_w} \\ B^2C_M'\chi_{M_w} \end{bmatrix} w_i^s(t) = \frac{1}{2}\rho U \Delta L \boldsymbol{\chi}_i^w w_i^s \tag{22b}$$

where $u_i^s(t)$ and $w_i^s(t)$ are complex-valued sinusoidal wind fluctuations; χ_{D_u}, χ_{D_w}, χ_{L_u}, χ_{L_w}, χ_{M_u} and χ_{M_w} are admittance functions that are dependent on the reduced frequencies and deck configuration; C_D, C_L and C_M are the force coefficients of the mean drag, lift and pitching torques, respectively; $C_D' = \mathrm{d}C_D/\mathrm{d}\alpha$, $C_L' = \mathrm{d}C_L/\mathrm{d}\alpha$ and $C_M' = \mathrm{d}C_M/\mathrm{d}\alpha$ are their derivatives around the mean angle of attack; and $\boldsymbol{\chi}_i^u$ and $\boldsymbol{\chi}_i^w$ are the vectors of the admittance functions and force coefficients, respectively. Similar to the approach used for flutter derivatives, the admittances are approximated as rational functions:

$$\boldsymbol{\chi}_i^u = \mathbf{A}_{i,1}^u + \sum_{l=1}^{m_u} \frac{\mathrm{j}K\mathbf{A}_{i,l+1}^u}{\mathrm{j}K + d_l^u} \tag{23}$$

where $\mathbf{A}_{i,1}^u$, $\mathbf{A}_{i,l+1}^u$ and $d_l^u \geq 0$ are frequency-independent coefficients. Consequently, an inverse Fourier transform method can be applied to derive the time-domain buffeting forces:

$$\mathbf{F}_i^{bu} = \frac{1}{2}\rho U \Delta L \sum_{l=1}^{m_u+1} \mathbf{A}_{i,l}^u u_i^s - \frac{1}{2}\rho U \Delta L \sum_{l=1}^{m_u} \frac{d_l^u U}{B} \boldsymbol{\phi}_{i,l}^u \tag{24a}$$

where u_i^s represents the stationary longitudinal wind fluctuations at the i-th node. The additional variables $\boldsymbol{\phi}_{i,l}^u$ $(l = 1, \cdots, m_u)$ satisfy the following equation:

$$\dot{\boldsymbol{\phi}}_{i,l}^u = -\frac{d_l^u U}{B} \boldsymbol{\phi}_{i,l}^u + \mathbf{A}_{i,l+1}^u u_i^s \tag{24b}$$

In this manner, the nonstationary buffeting forces in Eq. (15) are described as following:

$$\mathbf{F}^b = \beta^u(t)\mathbf{F}^{bu} + \beta^w(t)\mathbf{F}^{bw} \tag{25a}$$

in which the following can be defined:

$$\mathbf{F}^{bu} = \frac{1}{2}\rho U \Delta L \sum_{l=1}^{m_u+1} \mathbf{A}_l^u \mathbf{u}^s - \frac{1}{2}\rho U \Delta L \sum_{l=1}^{m_u} \frac{d_l^u U}{B} \boldsymbol{\phi}_l^u \tag{25b}$$

$$\dot{\boldsymbol{\phi}}_l^u = -\frac{d_l^u U}{B} \boldsymbol{\phi}_l^u + \mathbf{A}_{l+1}^u \mathbf{u}^s \tag{25c}$$

where $\mathbf{A}_l^u$ are the partitioned diagonal matrices of $\mathbf{A}_{i,l}^u$ $(i = 1, \cdots, N)$. For conciseness, similar formulas for buffeting forces caused by vertical turbulence are not presented here; they can be obtained by replacing u with w.

Note that, owing to the lack of available unsteady aerodynamic force models for nonstationary winds, these forces are currently calculated by the simple expedient use of stationary routines based on the flutter

derivatives and admittance functions. This approach can yield satisfactory results in the context of slowly varying mean wind speeds [46, 47]. Nevertheless, reliable aerodynamic models specific to nonstationary wind conditions need to be developed in future studies.

3.4 State-space equations in modal coordinates

By using the modal-superposition method, the deck motions can be represented in modal coordinates as $\mathbf{X}_d = \boldsymbol{\Psi}\mathbf{q}$, where $\mathbf{q}$ is the modal coordinate vector for n modes of interest and $\boldsymbol{\Psi}$ is the modal shape matrix of dimensions $3N \times n$. The generalized dynamic equation is then derived as follows:

$$\mathbf{M}_q\ddot{\mathbf{q}} + \mathbf{C}_q\dot{\mathbf{q}} + \mathbf{K}_q\mathbf{q} = \mathbf{Q}^{se} + \beta^u\mathbf{Q}^{bu} + \beta^w\mathbf{Q}^{bw} \tag{26}$$

where $\mathbf{M}_q = \boldsymbol{\Psi}^{\mathrm{T}}\mathbf{M}_d\boldsymbol{\Psi}$, $\mathbf{C}_q = \boldsymbol{\Psi}^{\mathrm{T}}\mathbf{C}_d\boldsymbol{\Psi}$ and $\mathbf{K}_q = \boldsymbol{\Psi}^{\mathrm{T}}\mathbf{K}_d\boldsymbol{\Psi}$ are the modal mass, damping and stiffness matrices, respectively. The generalized motion-induced force vector $\mathbf{Q}^{se} = \boldsymbol{\Psi}^{\mathrm{T}}\mathbf{F}^{se}$ is given as follows:

$$\mathbf{Q}^{se} = \frac{1}{2}\rho U^2 \Delta L\left(\mathbf{A}_1^{se,q}\mathbf{q} + \frac{B}{U}\mathbf{A}_2^{se,q}\dot{\mathbf{q}} + \frac{B^2}{U^2}\mathbf{A}_3^{se,q}\ddot{\mathbf{q}} + \sum_{l=1}^{m_{se}}\mathbf{q}_l^{se}\right) \tag{27a}$$

$$\dot{\mathbf{q}}_l^{se} = -\frac{d_l^{se}U}{B}\mathbf{q}_l^{se} + \mathbf{A}_{l+3}^{se,q}\dot{\mathbf{q}} \tag{27b}$$

where $\mathbf{A}_l^{se,q} = \boldsymbol{\Psi}^{\mathrm{T}}\mathbf{A}_l^{se}\boldsymbol{\Psi}$ $(l = 1, \cdots, m_{se} + 3)$ are the generalized frequency-independent coefficients, and $\mathbf{q}_l^{se} = \boldsymbol{\Psi}^{\mathrm{T}}\boldsymbol{\phi}_l^{se}$ $(l = 1, \cdots, m_{se})$ are generalized additional variables to consider the unsteady effect of motion-induced forces. Similarly, the generalized buffeting force vectors $\mathbf{Q}^{bu} = \boldsymbol{\Psi}^{\mathrm{T}}\mathbf{F}^{bu}$ and $\mathbf{Q}^{bw} = \boldsymbol{\Psi}^{\mathrm{T}}\mathbf{F}^{bw}$ are expressed as follows:

$$\mathbf{Q}^{bu} = \frac{1}{2}\rho U\Delta L\sum_{l=1}^{m_u+1}\mathbf{A}_l^{u,q}\mathbf{u}^s - \frac{1}{2}\rho U\Delta L\sum_{l=1}^{m_u}\frac{d_l^u U}{B}\mathbf{q}_l^u \tag{28a}$$

$$\dot{\mathbf{q}}_l^u = -\frac{d_l^u U}{B}\mathbf{q}_l^u + \mathbf{A}_{l+1}^{u,q}\mathbf{u}^s \tag{28b}$$

where $\mathbf{A}_l^{u,q} = \boldsymbol{\Psi}^{\mathrm{T}}\mathbf{A}_l^u$ $(l = 1, \cdots, m_u + 1)$ and $\mathbf{q}_l^u = \boldsymbol{\Psi}^{\mathrm{T}}\boldsymbol{\phi}_l^u$ $(l = 1, \cdots, m_u)$.

By substituting the expressions for $\mathbf{Q}^{se}$ and $\mathbf{Q}^{bu}$ into the generalized dynamic equation, it is transformed to its state-space form:

$$\dot{\mathbf{Y}} = \boldsymbol{\mathcal{A}}(t)\mathbf{Y} + \boldsymbol{\mathcal{B}}_u(t)\mathbf{u}^{s,q} + \boldsymbol{\mathcal{B}}_w(t)\mathbf{w}^{s,q} \tag{29}$$

where $\mathbf{Y} = \left[\mathbf{q}^{\mathrm{T}} \quad \dot{\mathbf{q}}^{\mathrm{T}} \quad \mathbf{q}_1^{se\,\mathrm{T}} \quad \cdots \quad \mathbf{q}_{m_{se}}^{se\,\mathrm{T}} \quad \mathbf{q}_1^{u\,\mathrm{T}} \quad \cdots \quad \mathbf{q}_{m_u}^{u\,\mathrm{T}} \quad \mathbf{q}_1^{w\,\mathrm{T}} \quad \cdots \quad \mathbf{q}_{m_w}^{w\,\mathrm{T}}\right]^{\mathrm{T}}$; $\boldsymbol{\mathcal{A}}(t)$, $\boldsymbol{\mathcal{B}}_u(t)$ and $\boldsymbol{\mathcal{B}}_w(t)$ are matrices of deterministic time-varying coefficients; and $\mathbf{u}^{s,q} = \mathbf{A}^{u,q}\mathbf{u}^s$ and $\mathbf{w}^{s,q} = \mathbf{A}^{w,q}\mathbf{w}^s$ are generalized stationary fluctuations with $\mathbf{A}^{u,q} = \left[\mathbf{A}_1^{u,q\,\mathrm{T}} \quad \cdots \quad \mathbf{A}_{m_u+1}^{u,q\,\mathrm{T}}\right]^{\mathrm{T}}$ and $\mathbf{A}^{w,q} = \left[\mathbf{A}_1^{w,q\,\mathrm{T}} \quad \cdots \quad \mathbf{A}_{m_w+1}^{w,q\,\mathrm{T}}\right]^{\mathrm{T}}$. The spectral density matrices for $\mathbf{u}^{s,q}$ and $\mathbf{w}^{s,q}$ are given by the following:

$$\mathbf{S}_{\mathbf{u}^{s,q}} = S_u\mathbf{A}^{u,q}\boldsymbol{\mathcal{C}}_{\mathbf{u}}(\mathbf{A}^{u,q})^{\mathrm{T}} \tag{30a}$$

$$\mathbf{S}_{\mathbf{w}^{s,q}} = S_w\mathbf{A}^{w,q}\boldsymbol{\mathcal{C}}_{\mathbf{w}}(\mathbf{A}^{w,q})^{\mathrm{T}} \tag{30b}$$

where S_u and S_w are PSDs of the derived stationary turbulences in the longitudinal and vertical directions, respectively. $\boldsymbol{\mathcal{C}}_{\mathbf{u}}$ and $\boldsymbol{\mathcal{C}}_{\mathbf{w}}$ are time-invariant coherence function matrices used to consider the spanwise correlation of wind fluctuations, of which the (i, j) entry is defined as follows:

$$\mathrm{Coh}(x_i, x_j, \omega) = \exp\left(-\frac{c_u \omega |x_i - x_j|}{2\pi \max[\bar{U}(t)]}\right) \tag{31}$$

where x_i is the spanwise coordinate of the i-th node, and c_u is the decay coefficient for longitudinal turbulence. Note that the correlation of the longitudinal and vertical turbulences is disregarded.

3.5 Statistical moment equations of nonstationary buffeting responses

The stationary Gaussian processes $\mathbf{u}^{s,q}$ and $\mathbf{w}^{s,q}$ are approximated individually by multivariate OU processes, i.e., $\mathbf{u}^{s,q} \approx \mathbf{Z}^u(t)$ and $\mathbf{w}^{s,q} \approx \mathbf{Z}^w(t)$, which satisfy the stochastic differential equation:

$$\mathrm{d}\mathbf{Z}^u(t) = -\boldsymbol{\alpha}^u \mathbf{Z}^u(t)\mathrm{d}t + \boldsymbol{\Theta}^u \mathrm{d}\mathbf{W}^u(t) \tag{32a}$$

$$\mathrm{d}\mathbf{Z}^w(t) = -\boldsymbol{\alpha}^w \mathbf{Z}^w(t)\mathrm{d}t + \boldsymbol{\Theta}^w \mathrm{d}\mathbf{W}^w(t) \tag{32b}$$

where $\boldsymbol{\alpha}^u$, $\boldsymbol{\Theta}^u$, $\boldsymbol{\alpha}^w$ and $\boldsymbol{\Theta}^w$ are the corresponding coefficient matrices, and $\mathbf{W}^u$ and $\mathbf{W}^w$ are the corresponding Wiener processes, which are mutually independent.

By substituting Eq. (32) into Eq. (29), the augmented states are written as follows:

$$\mathrm{d}\begin{bmatrix}\mathbf{Y}\\ \mathbf{Z}^u\\ \mathbf{Z}^w\end{bmatrix} = \begin{bmatrix}\boldsymbol{\mathcal{A}} & \boldsymbol{\mathcal{B}}_u & \boldsymbol{\mathcal{B}}_w\\ \mathbf{0} & -\boldsymbol{\alpha}^u & \mathbf{0}\\ \mathbf{0} & \mathbf{0} & -\boldsymbol{\alpha}^w\end{bmatrix}\begin{bmatrix}\mathbf{Y}\\ \mathbf{Z}^u\\ \mathbf{Z}^w\end{bmatrix}\mathrm{d}t + \begin{bmatrix}\mathbf{0} & \mathbf{0}\\ \boldsymbol{\Theta}^u & \mathbf{0}\\ \mathbf{0} & \boldsymbol{\Theta}^w\end{bmatrix}\mathrm{d}\begin{bmatrix}\mathbf{W}^u\\ \mathbf{W}^w\end{bmatrix} \tag{33}$$

This equation is recognized as an Itô-type stochastic differential equation of the following form:

$$\mathrm{d}\mathbb{Y}(t) = \mathbf{g}(\mathbb{Y}(t), t)\mathrm{d}t + \mathbf{h}(\mathbb{Y}(t), t)\mathrm{d}\mathbf{W} \tag{34}$$

where $\mathbb{Y} = [\mathbf{Y}^{\mathrm{T}} \quad \mathbf{Z}^{u\mathrm{T}} \quad \mathbf{Z}^{w\mathrm{T}}]^{\mathrm{T}}$ is the augmented state vector and $\mathbf{W} = [\mathbf{W}^{u\mathrm{T}} \quad \mathbf{W}^{w\mathrm{T}}]^{\mathrm{T}}$.

The statistical moment equation for bridge buffeting can subsequently be derived as a set of first-order differential equations of the same form as Eq. (12) by following the procedure outlined in Section 2.3.

Note that the engagement of motion-induced forces renders the overall damping and stiffness matrices asymmetric; this results in a complex modal analysis if a time-domain or frequency-domain method is used. The MDOF model reveals that in the presence of the aerodynamic effect, the rotational center may shift upstream or downstream, as shown by Figure 12 from [60] and is closely associated with the downwash effect of aerodynamics [61]. The shift in the rotational center causes the vertical motions to be polluted by torsion, leading to fully coupled modes and, consequently, complex-valued modal frequencies and shapes. The detailed illustrations can be found in Appendix A. Apparently, these effects cannot be simply explained by SDOF models. Instead, in this study, an MDOF model is proposed to avoid complex modal analyses, and a stochastic calculus-based method is used to solve the multimode vibrations more efficiently.

In the context of nonstationary wind, time-varying mean wind speeds cause variations in kinetic pressure, leading to time-varying aerodynamic damping ratios and stiffness. This results in a distinctly time-varying aero-structural coupled system. Traditional frequency-domain approaches assume that the system is fixed within short windows, reducing the problem to time-invariant systems subjected to stationary excitations, as in the work of [17]. The entanglement of the asymmetric aerodynamic matrices with LTV systems further complicates the calculation since complex eigenvalue analysis will need to be conducted in each time window to update the real-time modal information. However, this assumption is valid only for slowly varying mean wind conditions and requires a CQC method due to asymmetry, resulting in further intensive calculations.

In contrast, the proposed method does not involve the above difficulties. It effectively accounts for the features of coupled DOFs and structural modes in long-span bridges by incorporating partially correlated

Ornstein-Uhlenbeck (OU) processes; these processes capture the interaction of modes via coefficients $\boldsymbol{\alpha}$ (drift) and $\boldsymbol{\Theta}$ (diffusion). Instead of proceeding to complex eigenvalue analyses, the method pivots its basis to Itô's lemma, which is equivalent to the Fokker-Planck equation with time-varying coefficients; this inherently addresses the time-varying characteristics owing to the coupling of nonstationary aerodynamic forces and structures, and subsequently establishes the moment evolution equation directly without further assumptions.

While the application of Itô's formula provides a novel and effective approach for analyzing nonstationary wind effects in structural engineering, several limitations should be considered. First, the accuracy of the results depends heavily on the quality of the wind speed data, particularly the statistical properties, including time-varying mean wind speeds and time modulation functions; these properties may significantly vary across different environments and different time-frequency analysis techniques. Furthermore, the computational complexity increases with the number of DOFs in the system, potentially limiting its application to very large or highly complex structures. Additionally, the assumptions made in nonstationary aerodynamics modeling, such as the linearity and Gaussian nature of the loading, may not fully capture the real-world complexities of wind-structure interactions. These limitations should be addressed in future research by developing more advanced models that can accommodate the nonlinearities and non-Gaussian behaviors and improve the efficiency of computational algorithms.

4 Numerical applications

With the established theoretical foundation, this section provides the calculation of the bridge buffeting response under various wind scenarios. The method is first validated through a two-step procedure, followed by discussions on the physical insights gained from the analysis of multimode nonstationary buffeting.

4.1 Stationary wind excitation and buffeting responses

Given the current limitations in available methods for directly validating nonstationary vibrations in MDOF systems, a step-by-step validation approach is adopted to demonstrate the reliability of the proposed state augmentation method. The reliability of the proposed method includes two key aspects: its reliability in investigating nonstationary vibration problems and its effectiveness in handling multi-DOF vibration problems. The first aspect has been demonstrated in a previous study [45] by simulating the nonstationary buffeting of a single-DOF system under nonstationary wind conditions, where nonstationary vibrations were validated using the Monte Carlo method and the pseudo excitation method. To validate the second aspect and assess the computational efficiency, the proposed approach is applied to compute the multimode vibrations of a model bridge excited by stationary turbulence. The results are compared to those obtained using the well-established frequency domain method (FDM) [62]. Note that the validation for the nonstationary case justifies its ability to address time-varying modes; thus, the validated effectiveness is not affected by the number of DOFs considered. The validation for the MDOF case justifies its reliability in reproducing mode-coupling effects and correlated loadings, and the validated effectiveness is independent of whether the problem is stationary. For conciseness, a further consolidated validation of a 2-DOF nonstationary problem is provided in Appendix B. Real-world nonstationary buffeting simulations are presented in the subsequent section.

As illustrated in Figure 3, the bridge has a deck width of $49.7\ \mathrm{m}$ and a main span of $1666\ \mathrm{m}$. In the interest of simplicity and generality, only the first symmetric torsional mode and a prior symmetric vertical

mode of the first order (two modes in total, producing moment equations of dimension 26) are considered, with modal frequencies of $n_1^{SV} = 0.1049$ Hz and $n_1^{ST} = 0.2987$ Hz, respectively, based on modal analysis results. To enhance the robustness of the validation, an additional calculation model that considers the first asymmetric torsional and vertical modes has been included, and the corresponding modal frequencies are $n_1^{AV} = 0.0858$ Hz and $n_1^{AT} = 0.266$ Hz. The static force coefficients and their derivatives are experimentally measured at zero angle of attack and are defined as follows: $C_D = 0.825$, $C_L = -0.048$, $C_M = 0.011$, $C_L' = 3.158$ and $C_M' = 0.367$.

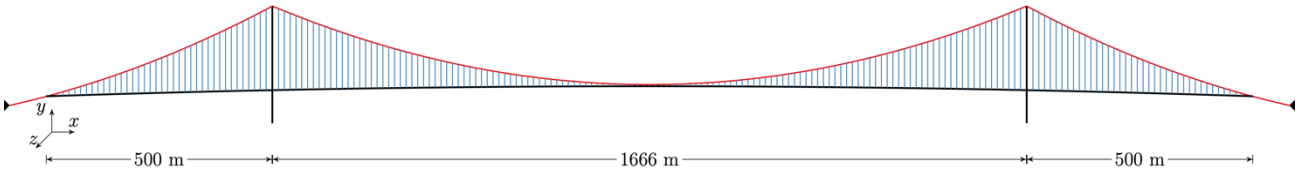

Fig. 3. Model of the long-span suspension bridge.

For the stationary wind field, Von Kármán- and Panofsky-type spectra are adopted to represent the longitudinal and vertical wind turbulence, respectively. The corresponding turbulence intensities of I_u and I_w are assumed to be 0.1, and the turbulence integral lengths $L_u = 76.4$ m and $L_w = 16.9$ m are obtained using the formulas given in [7]. The turbulence coherence decay coefficients $c_u = c_w = 10$ are adopted. A series of mean wind speed cases, ranging from 10 m/s to 45 m/s, are examined to validate the results.

Calibration of the coefficient matrices $\boldsymbol{\alpha}$ and $\boldsymbol{\Theta}$ is a crucial step in the SAM, allowing OU processes to accurately represent the generalized stationary fluctuations, e.g., $\mathbf{u}^{s,q}$. The total buffeting responses are influenced primarily by two factors: the resonant response and the background response. The value of $\boldsymbol{\alpha}$ can be determined by fitting $\mathbf{S}_{\mathbf{u}^{s,q}}$ and $\mathbf{S}_{\mathbf{Z}^u}$ at the modal frequencies because of the narrowband characteristics of the resonant response. Note that the engagement of the motion-induced forces slightly altered the natural frequencies, as illustrated in Appendix A, and the fitting at the on-wind natural frequencies is considered a further improvement. $\boldsymbol{\Theta}$ can then be found by ensuring that the autocovariance matrices of $\mathbf{Z}^u$ and $\mathbf{u}^{s,q}$ match, thereby ensuring an accurate background response. The comparison between each component of $\mathbf{S}_{\mathbf{u}^{s,q}}$ and $\mathbf{S}_{\mathbf{Z}^u}$ of the fitted OU processes for the symmetric mode case is shown in Figure 4 for a mean wind speed $U = 40$ m/s.

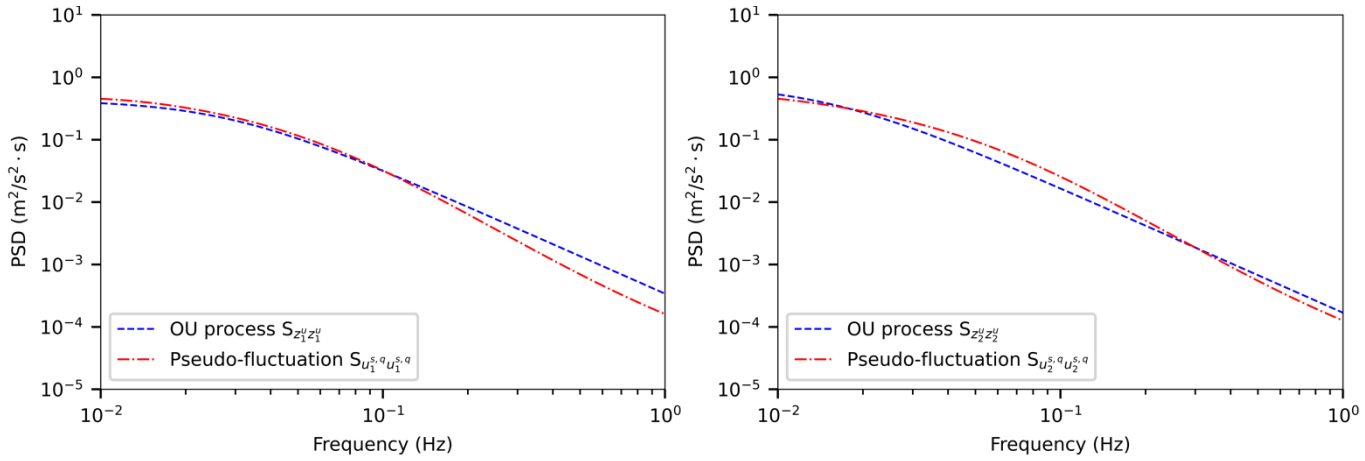

(a) PSD of the first fluctuation component

(b) PSD of the second fluctuation component

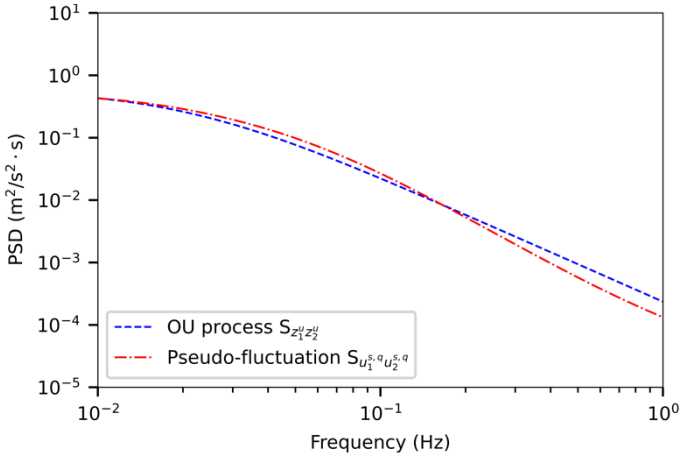

(c) Cross PSD of the fluctuation components

Fig. 4. PSD comparisons between the generalized stationary fluctuations and the fitted OU processes.

The root mean square (RMS) results for the vertical and rotational displacements of the deck at the midspan for symmetric-modal vibrations are displayed in Figure 5; the responses at the quarter span for asymmetric-modal vibrations obtained using the proposed SAM and the classical FDM are also included. The results from the classical FDM are obtained by integrating stationary response spectra across 500 frequency points.

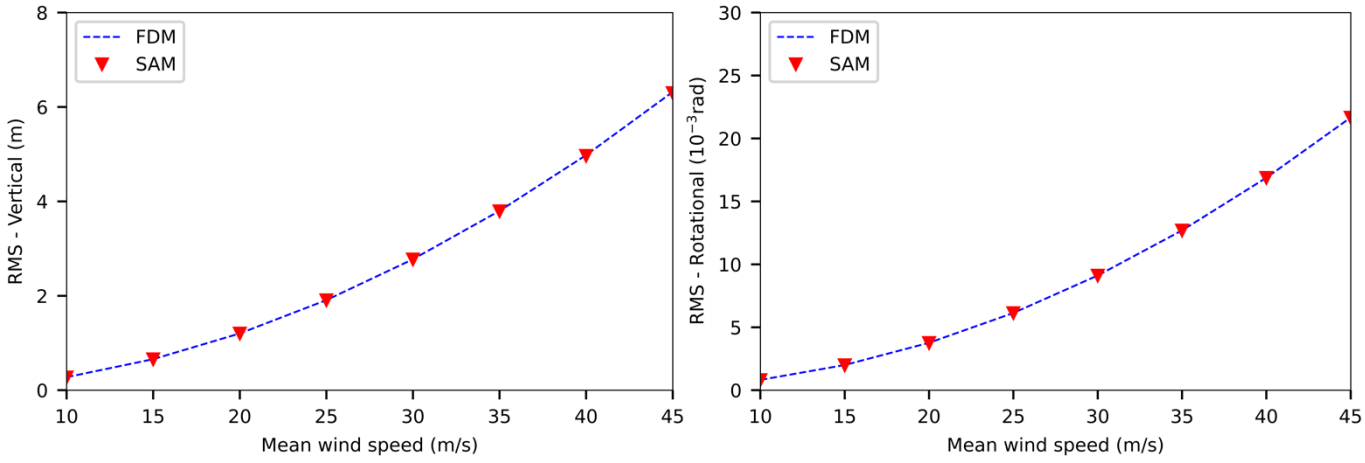

(a) Vertical displacement (Symmetric)

(b) Rotational displacement (Symmetric)

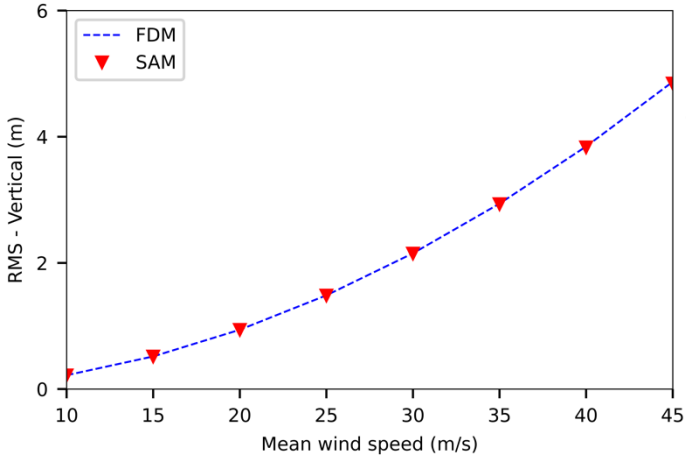

(c) Vertical displacement (Asymmetric)

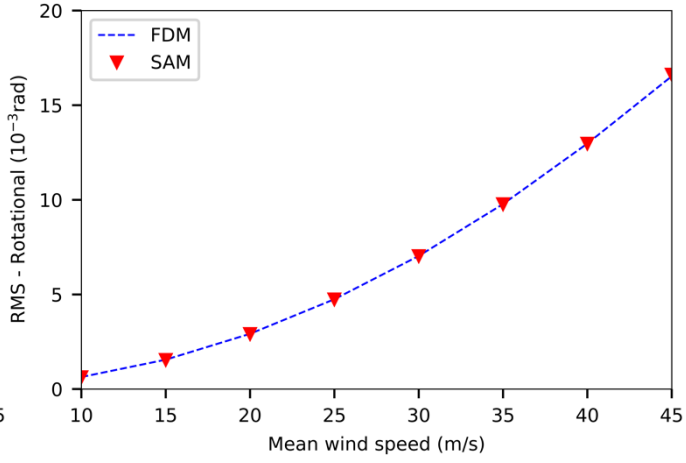

(d) Rotational displacement (Asymmetric)

Fig. 5. Comparisons of the RMS vertical and rotational displacement responses of the deck at the mid-span for symmetric-modal vibrations and at the quarter-span for asymmetric-modal vibrations, as calculated by SAM and FDM.

As shown in Figure 5, the results obtained by SAM and by FDM agree very well, demonstrating the reliability of the SAM in determining the buffeting response. Additionally, SAM shows a significant computational efficiency advantage over FDM. In this study, an Intel Core i7 4-Core computer with 16 GB of RAM and a maximum frequency of 3.4 GHz is used. SAM required an average computing time of 3.4 s, whereas the average computing time for FDM (without parallel computing) was approximately 434 s. The entire running time of FDM is approximately proportional to the number of frequencies because its major effort is used in the determination of the response spectra at each discrete frequency. In contrast, SAM enables the immediate calculation of the response moments by solving the moment equations only once.

4.2 Nonstationary wind excitation and buffeting responses

In this section, the SAM is applied to calculate the responses of the model bridge under realistic nonstationary wind conditions, which consist of a time-varying mean and uniformly time-modulated fluctuations. To demonstrate the method's capabilities, the first symmetric torsional mode and the three previous symmetric vertical modes (four modes in total, giving moment equations of dimension 100) are considered, and the frequencies for the second and third vertical modes are as follows: $n_2^{SV} = 0.1366$ Hz and $n_3^{SV} = 0.2256$ Hz, respectively. The flutter derivatives used in the analysis are derived from wind tunnel experiments [63].

The nonstationary wind speed model is derived from the Typhoon Hagupit record, which was measured in China during its passage in September 2008. During the typhoon, a high-precision 3-axis ultrasonic anemometer was used to record wind speed data at a frequency of 10 Hz over a 24-hour period, from 18:00 on the 23rd to 18:00 on the 24th (GMT+8). The details of these measurements are provided in [64, 65]. Three orthogonal wind fluctuation components and mean wind speeds were extracted from the collected data. The vertical turbulence was assumed to follow a zero-mean distribution, and the longitudinal wind component was aligned perpendicular to the bridge axis. The time history of the longitudinal wind speed is shown in Figure 6. To represent the nonstationary characteristics of Typhoon Hagupit well, two segments (12-13 h and 19-20 h) are selected for buffeting analysis. Detailed time histories of these wind segments are provided in Figure 7; here, the data reveals a steadily increasing trend in the first segment and a periodically changing trend in the second segment.

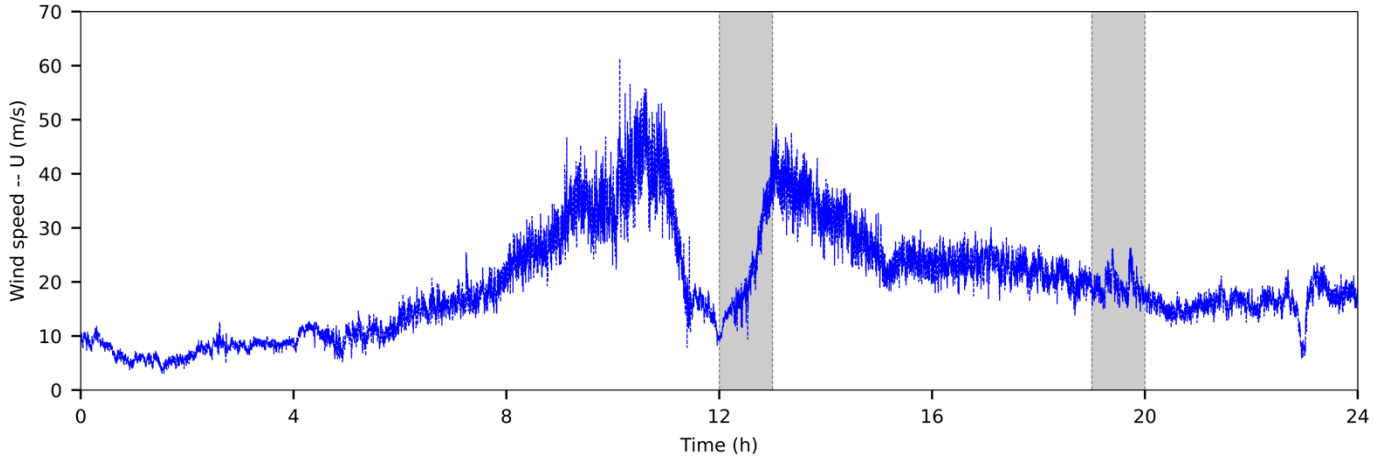

Fig. 6. Time history of the longitudinal wind speed of the recorded Typhoon Hagupit in September 2008.

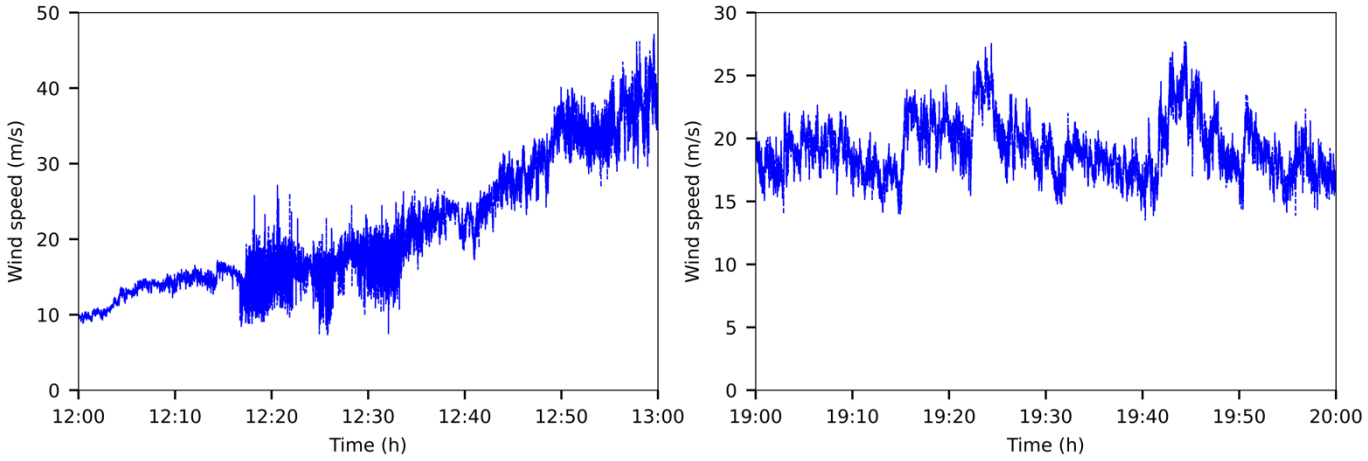

(a) 12-13 h (b) 19-20 h

Fig. 7. Time histories of the longitudinal wind speed of the selected segments of the Typhoon Hagupit record.

The discrete wavelet transform (DWT) [6] is used to extract the time-varying mean wind speed $\bar{U}(t)$ and zero-mean nonstationary fluctuations $u(t)$ and $w(t)$. The order 20 Daubechies wavelet (db20) with a 10-level decomposition is employed in this process. Figure 8 shows the derived time-varying mean wind speeds and zero-mean nonstationary fluctuations for both wind segments. The higher cutoff frequencies of the mean wind speeds are approximately 0.005 Hz; this value is significantly lower than the primary frequency of the concerned bridge modes (0.1049 Hz) and justifies the consideration of slowly varying mean wind speeds in kinetic pressure. The solid red lines in Figure 8 (c)-(f) represent the time-varying standard deviations of the nonstationary fluctuations, $\sigma_u(t)$ and $\sigma_w(t)$, and the estimation process is detailed below.

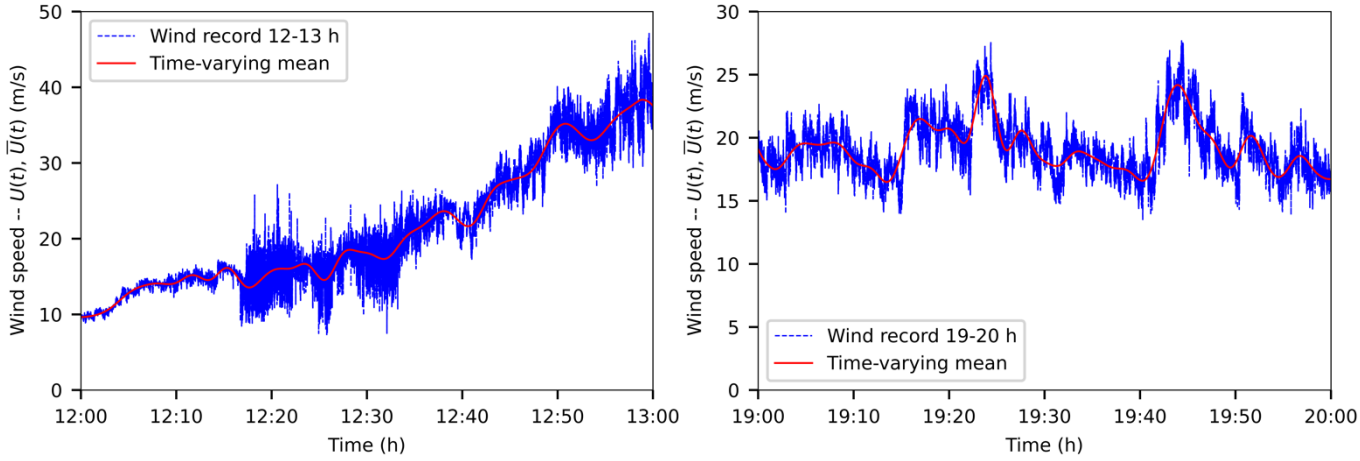

(a) Time-varying mean, 12-13 h

(b) Time-varying mean, 19-20 h

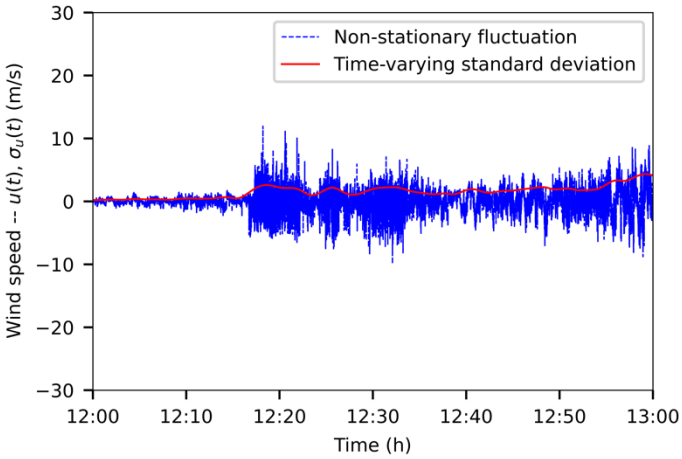

(c) Nonstationary longitudinal fluctuations, 12-13 h

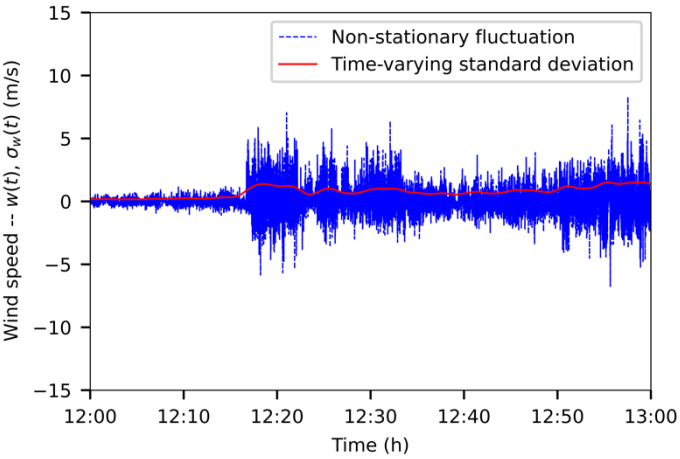

(d) Nonstationary vertical fluctuations, 12-13 h

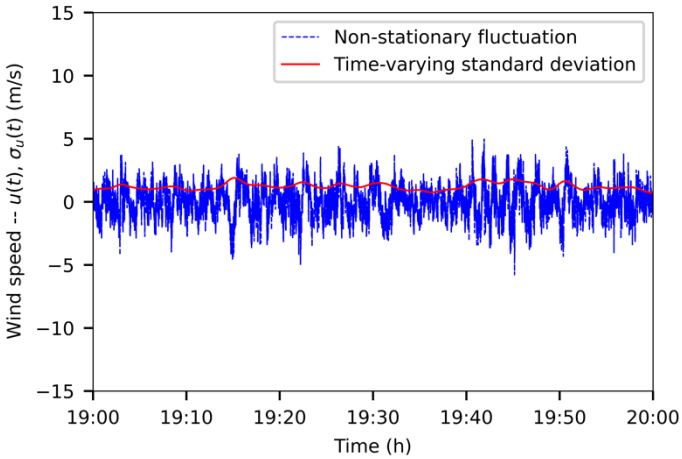

(e) Nonstationary longitudinal fluctuations, 19-20 h

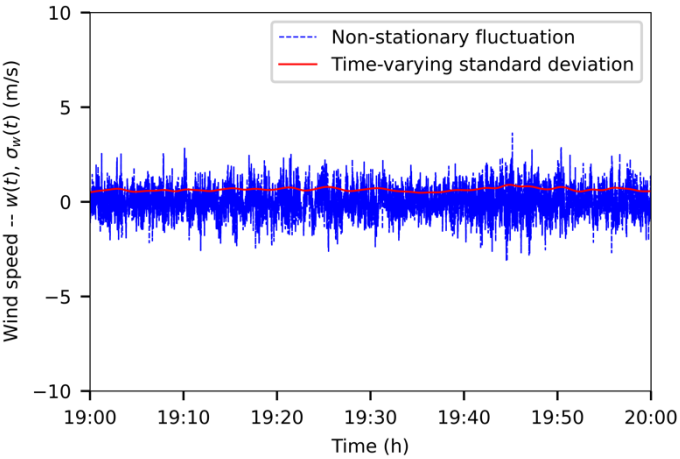

(f) Nonstationary vertical fluctuations, 19-20 h

Fig. 8. Wind speed model extracted from the selected wind segments from the Typhoon Hagupit record.

The extracted nonstationary fluctuations are represented using the uniformly time-modulated model, where the modulation function $\beta(t)$ is simplified as the normalized standard deviation [14], e.g., $\sigma_u(t)/\sigma_{u,\max}$. The standard deviation $\sigma_u(t)$ is estimated using the Nadaraya-Watson estimator and the kernel regression method [6, 66]:

$$\sigma_u^2(t) = \frac{\sum_{i=1}^{N}[u(t_i)]^2 K_\delta(t-t_i)}{\sum_{i=1}^{N} K_\delta(t-t_i)} \tag{35}$$

where the kernel $K_\delta(t) = \left(\frac{1}{\sqrt{2\pi}\delta}\right)\exp\left(-\frac{t^2}{2\delta^2}\right)$ is a Gaussian function scaled by a bandwidth δ and N is the total number of data points. The estimation results are plotted as solid curves in Figure 8 (c)-(f). The derived stationary fluctuation is obtained as follows:

$$u^s(t) = \frac{u(t)}{\beta_u(t)} \tag{36}$$

The PSD of $u^s(t)$ is estimated using Welch's method, which provides a frequency resolution of 0.0024 Hz. To account for the possibility that the PSD of $u^s(t)$ may not comply with widely used wind spectra, a general spectrum form [6, 67] is adopted to fit the PSD estimate:

$$S_{u^s}(n) = \frac{6u_*^2 A}{(1+Bn^{d_1})^{d_2}} \tag{37}$$

where $6u_*^2$ corresponds to the variance of the fluctuations, A, B, d_1 and d_2 are fitting parameters and n is the frequency. The fitted parameters for each case are listed in Table 1.

Table 1. The estimated parameters in Eq. (36) for each wind segment.

Case	u_* (m/s)	A	B	d_1	d_2	$-d_1 d_2$
u^s, 12-13 h	1.696	11.19	17.76	1.05	1.779	-1.868
w^s, 12-13 h	0.638	2.7	2.27	0.981	2.385	-2.34
u^s, 19-20 h	0.759	21.86	38.33	1.165	1.725	-2.01
w^s, 19-20 h	0.364	8.0	11.71	1.03	1.678	-1.728

Figure 9 displays the time histories of $u^s(t)$, and the corresponding PSD estimates with fitted wind spectra are presented in Figure 10. As shown, the spectral slopes in the high-frequency region roughly align with the Kolmogorov slope of $-5/3$; this result is consistent with the analysis in [6].

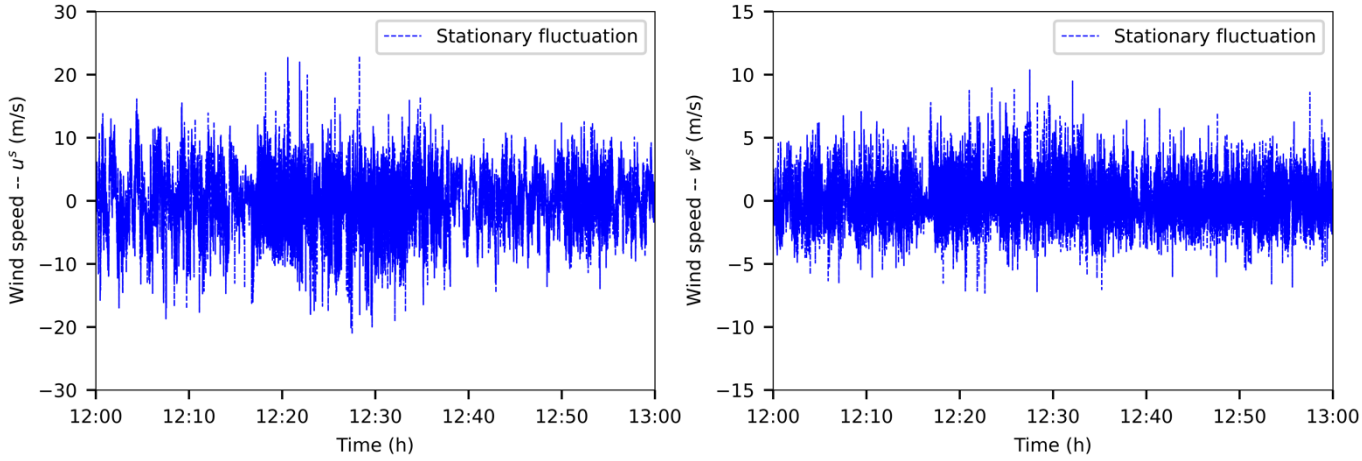

(a) Longitudinal wind, 12-13 h (b) Vertical wind, 12-13 h

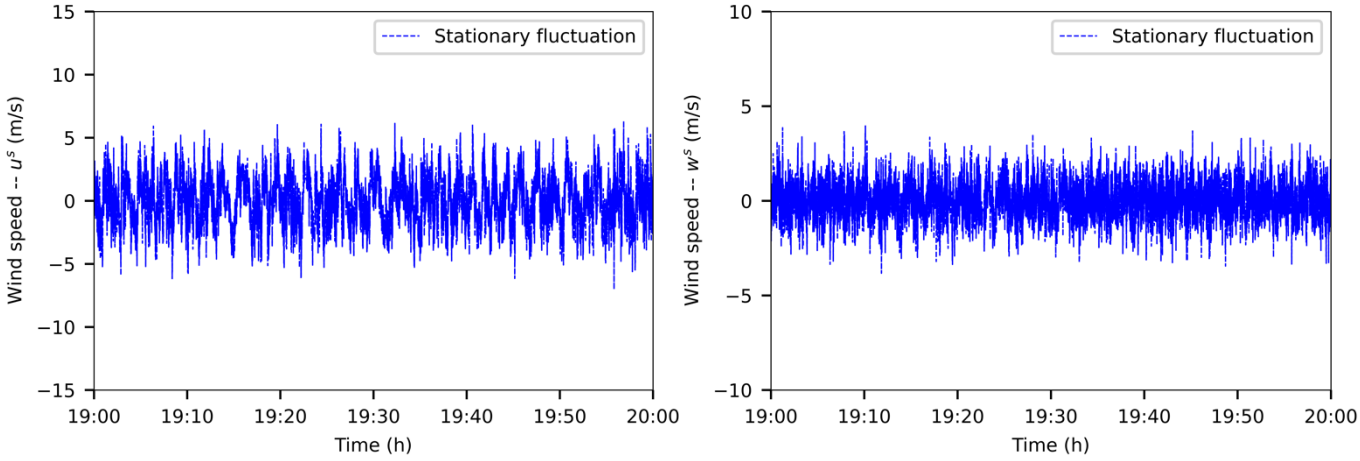

(c) Longitudinal wind, 19-20 h (d) Vertical wind, 19-20 h

Fig. 9. Time histories of the derived stationary fluctuations.

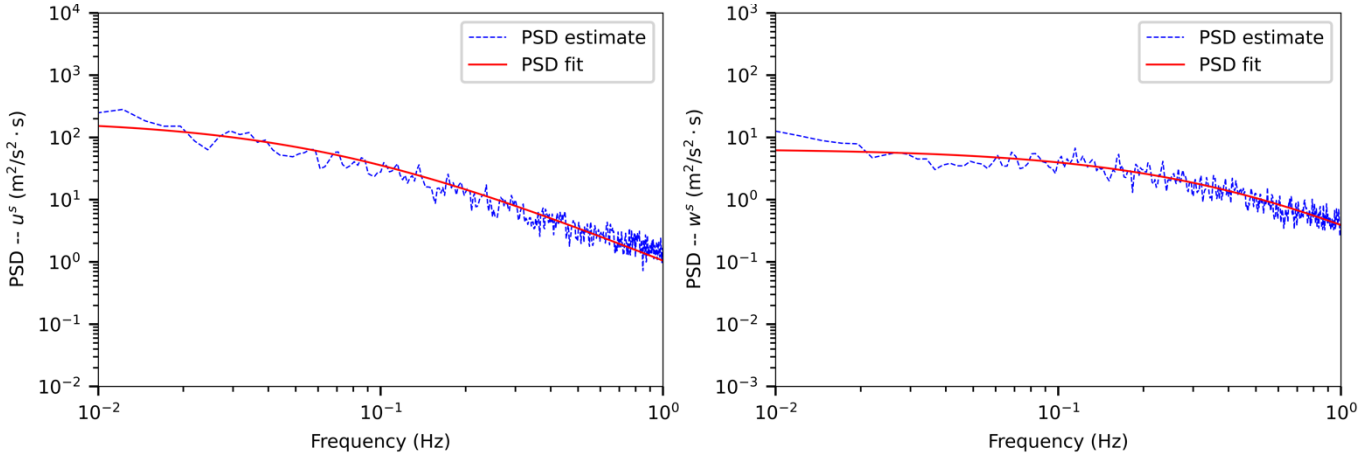

(a) Longitudinal wind, 12-13 h (b) Vertical wind, 12-13 h

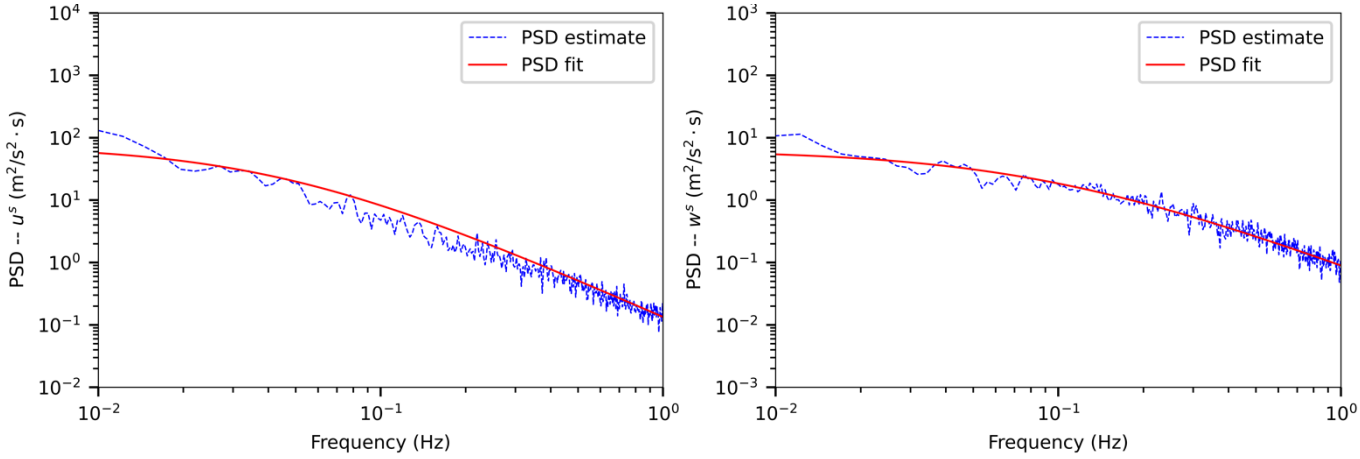

(c) Longitudinal wind, 19-20 h (d) Vertical wind, 19-20 h

Fig. 10. PSD estimates and the fitted PSD of the derived stationary fluctuations.

As in the previous verification, the coefficient matrices $\boldsymbol{\alpha}$ and $\boldsymbol{\Theta}$ are calibrated to match the generalized stationary fluctuations. The calibration results of $\mathbf{S}_{\mathbf{Z}^u}$ and $\mathbf{S}_{\mathbf{Z}^w}$ and their comparisons with $\mathbf{S}_{\mathbf{u}^{s,q}}$ and $\mathbf{S}_{\mathbf{w}^{s,q}}$ are omitted for brevity. Figure 11 shows the time-varying RMSs of the vertical and rotational displacements of the deck at the midspan for each wind segment case. The bridge is assumed to be initially at rest when

subjected to each wind segment. For comparison, the traditional time-frequency analysis technique is further used to calculate stationary responses in each subdivided 10-minute window by treating each wind segment as stationary.

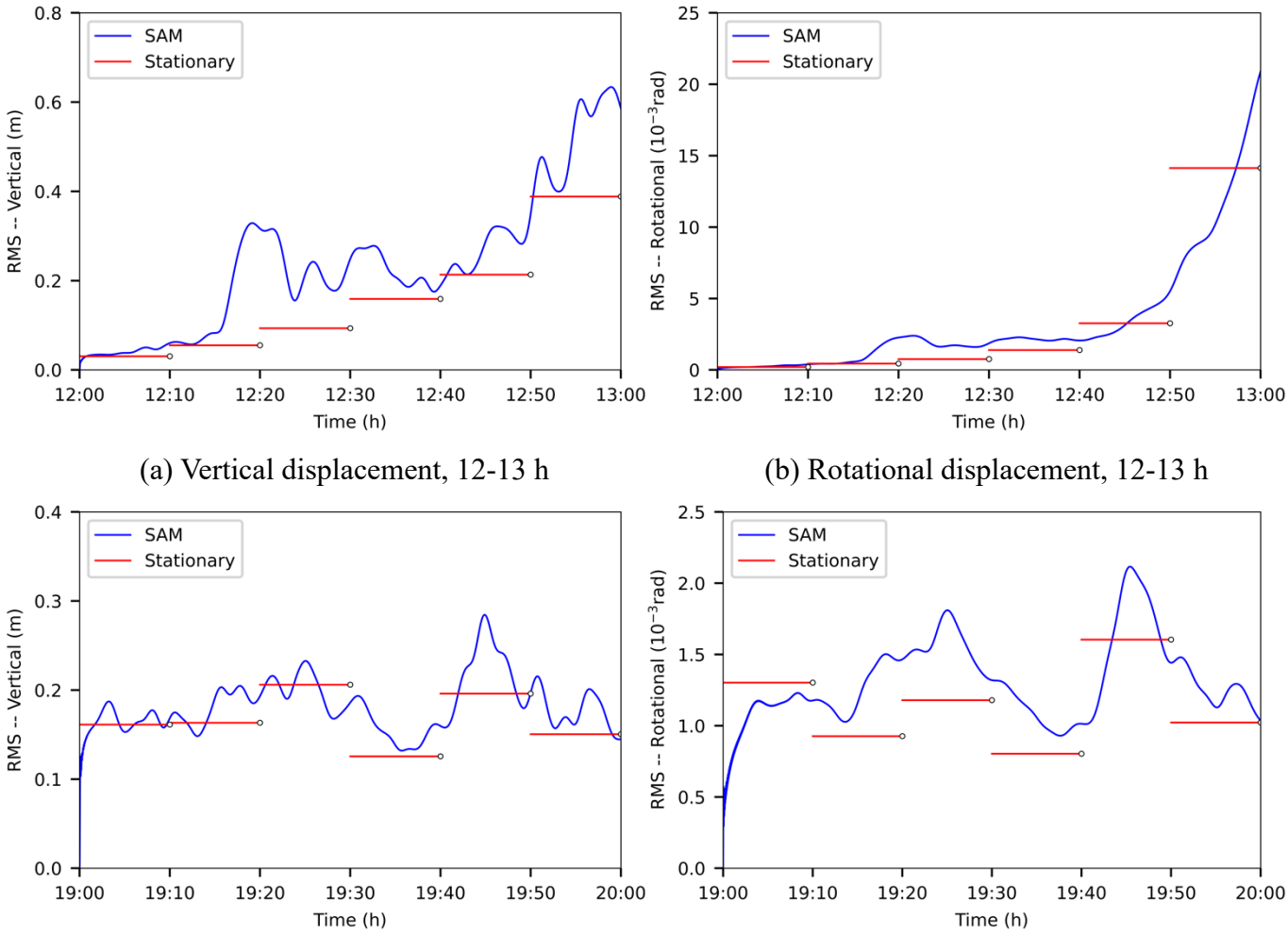

(a) Vertical displacement, 12-13 h

(b) Rotational displacement, 12-13 h

(c) Vertical displacement, 19-20 h

(d) Rotational displacement, 19-20 h

Fig. 11. Time-varying RMSs and stationary RMSs of the displacement responses of the bridge deck at the midspan under excitation of Typhoon Hagupit.

As illustrated in Figure 11, the RMS results vary significantly over time, exhibiting pronounced nonstationary characteristics. The trend in variation closely follows that of the corresponding mean wind speed since the time-varying mean wind speed directly amplifies or attenuates the excitation intensity. This also affects the motion-induced forces, causing variations in aerodynamic damping and partially accounting for the observed trend similarity.

Moreover, significant discrepancies are noted between stationary and nonstationary responses in each window. The initial responses to each wind segment from the stationary results are consistently greater than those of the nonstationary responses, which are more pronounced in Figure 11 (c) and (d); this is likely caused by a lack of "build-up" time for nonstationary vibrations to reach a stationary state, as reported by several studies [18, 22]. However, since the stationary analysis overlooks the peak of nonstationary excitations, the nonstationary response steadily increases as energy accumulates and eventually surpasses the stationary result. A noticeable discrepancy in the vertical displacement results from 12:10~12:20 h is that the nonstationary

response is nearly four times greater than the stationary response. Field measurements [64] and wind record data indicate substantial changes in the wind speed and direction during the passage of the typhoon eye at approximately 12:00 h, with an almost complete reversal of the wind direction after landfall.

To better illustrate the changes during eye passage, Figure 12 shows detailed time histories of nonstationary longitudinal and vertical winds from 12:10 h to 12:20 h, along with time-varying mean wind speeds and zero-mean nonstationary fluctuations derived via time-frequency analysis. The wind speed clearly exhibits significant non-stationarity and non-homogeneity; here, the wind remains calm until the speed drastically changes at approximately 12:16 h.

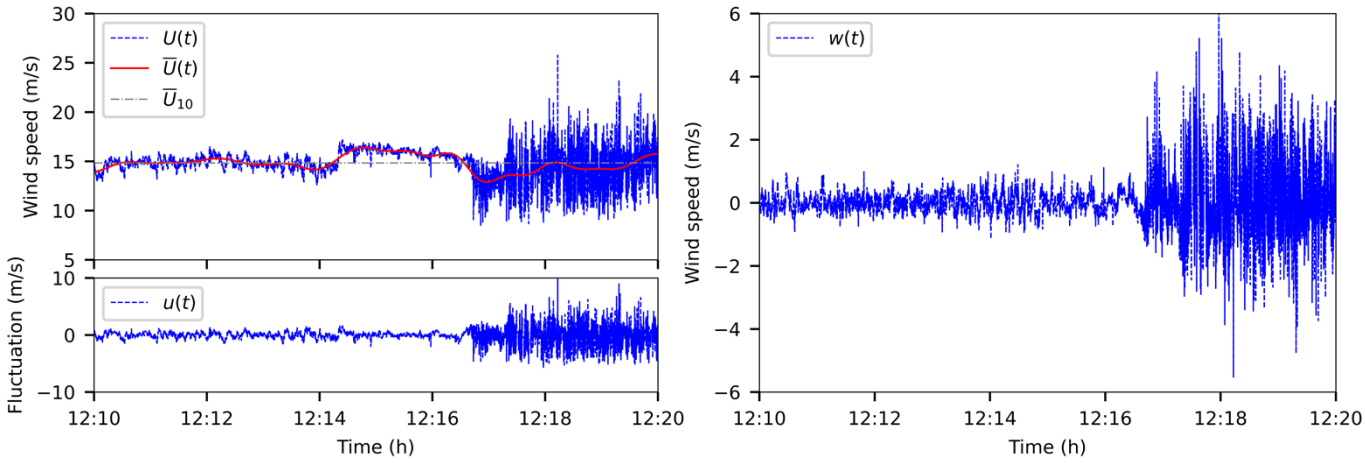

(a) Longitudinal wind (b) Vertical wind

Fig. 12. Time histories of the longitudinal and vertical wind speeds recorded during Typhoon Hagupit from 12:10 h to 12:20 h.

A detailed study on multimode buffeting under Typhoon Hagupit from 12:10~12:20 h is conducted using the SAM. The first symmetric and asymmetric torsional modes, along with all prior vertical modes, are considered (seven modes in total, giving moment equations of dimension 301) to ensure comprehensive results. Figure 13 shows the RMS results of the nonstationary vertical and rotational displacements of the deck at the midspan and quarter span. Stationary responses obtained using the FDM are also provided for comparison. Additionally, the computational efficiency of the proposed SAM in relation to system dimensions is provided in Table 2. Note that, to be comparable the computation time is estimated for the simulation over 0~600 s.

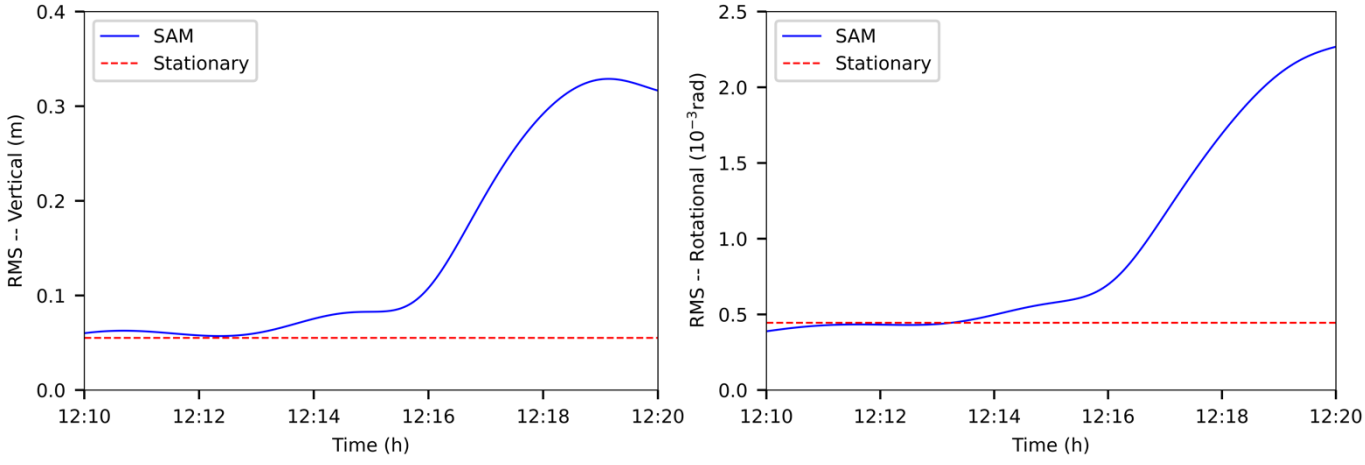

(a) Vertical displacement (mid-span) (b) Rotational displacement (mid-span)

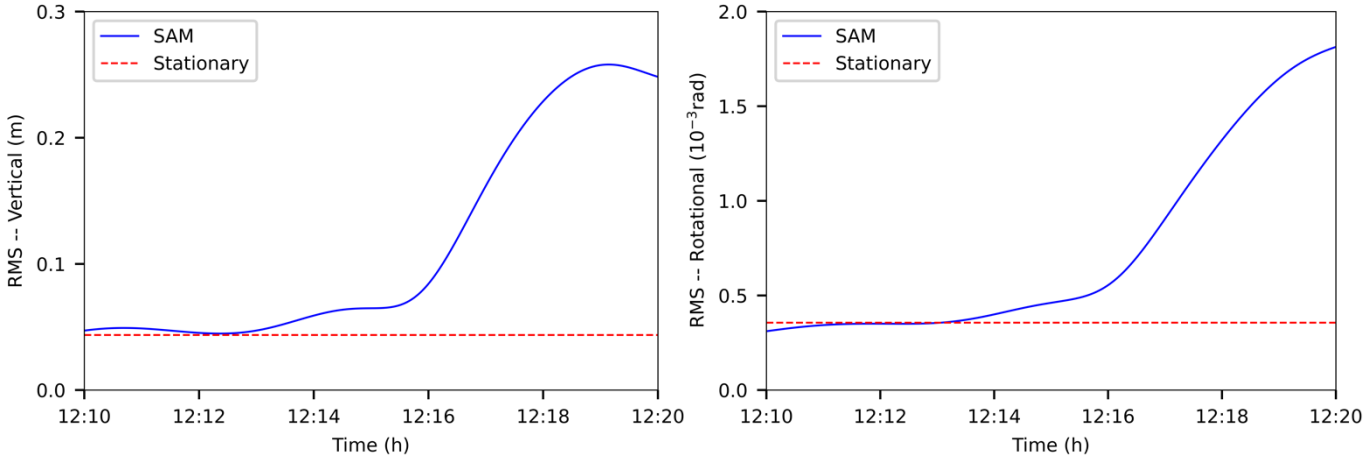

(c) Vertical displacement (quarter-span) (d) Rotational displacement (quarter-span)

Fig. 13. Time-varying RMS and stationary RMS displacement responses of the bridge deck at the midspan and quarter span under the excitation of Typhoon Hagupit from 12:10 h to 12:20 h.

Table 2. Computational time required for the SAM with respect to system dimensions

System dimension	2 DOFs	4 DOFs	7 DOFs
Size of moment equations	26	100	301
Time	3.4 s	238 s	2451 s

As shown in Figure 13, nonstationary responses initially align with stationary responses because of the weak nonstationary characteristics of the wind speed from 12:10 h to 12:16 h. However, as the wind speed drastically changes during eye passage, the nonstationary response continues to increase, ultimately becoming four times greater than the stationary result. In the stationary buffeting analysis, the transition in wind speed development is disregarded by treating the entire 10-minute segment as a stationary process. This introduces the effect of peak clipping by averaging the wind load, potentially overlooking nonstationary excitation peaks and leading to lower responses. For transient extreme wind events such as downbursts, simple stationarity treatment may yield conservative results [45], whereas for long-running nonstationary winds such as typhoons, it may fail to capture true peak responses, resulting in potential risks.

5 Conclusion

In this work, a state augmentation approach for calculating the nonstationary vibrations of a long-span bridge under nonstationary wind is presented. This approach builds upon previous work relevant only to systems with a single DOF, extends it to multi-DOF systems and incorporates unsteady effects. The buffeting response is predicted by considering both the unsteady aerodynamic forces induced by nonstationary turbulence and structural motions. The aerodynamic-mechanical system is time-varying because of the changing mean wind speed, leading to nonstationary responses even in cases of stationary wind. Moreover, the involvement of motion-induced forces causes the system damping and stiffness matrices to be asymmetric, leading to coupled modal vibrations that cannot be sufficiently captured by SDOF models. The proposed MDOF approach is based on stochastic calculus, eliminates the need for complex modal analysis, which is typically required in coupled dynamics, and effectively explains the mechanism of the modal coupling effect.

The essential steps in the proposed approach are as follows. First, the Ornstein-Uhlenbeck process is employed to approximate the stationary excitations derived from the nonstationary excitations by adopting a

uniform time-modulation model. Second, the stochastic form of the buffeting differential equations is derived by assembling the OU excitations and system states into an augmented vector. Furthermore, by using Itô's formula, the stochastic buffeting equations are converted into a set of first-order differential equations that describe the evolution of response moments over time. The stars and bars approach, combined with symbolic calculations, enable the automatic generation of the moment equations for dynamic systems with any number of DOFs and for response moments of any order.

The effectiveness of the proposed method is demonstrated through comparisons with the well-established frequency domain method in a stationary vibration case. The FDM requires significant computational effort for spectrum operations across numerous discrete frequencies, whereas SAM is far more efficient. In the nonstationary vibration case, the results reveal significant variations in the RMS response over time, reflecting patterns in the time-varying mean wind speed. These results confirm that the proposed approach is capable of accurately capturing nonstationary features of the vibrations. These findings indicate that stationary buffeting analysis may yield conservative estimates for transient extreme wind events and fail to capture true peak responses for long-running nonstationary winds. The proposed state augmentation method, on the other hand, provides a more accurate analysis, enhancing safety and reliability in engineering practices.

Acknowledgements

The study was supported by the National Natural Science Foundation of China (grant Nos. 51978527, 52278520 and 52478552), the Natural Science Foundation of Shanghai (Grant No. 23ZR1464900), and the Fundamental Research Funds for the Central Universities (Grant No. 22120240363).

Appendix A

To illustrate the mode-coupling effect of a wind-induced vibration problem, the stationary vibrations of a two-mode bridge deck under stationary white-noise turbulence are investigated. The first symmetric vertical mode and the first symmetric torsional mode, i.e., $n_1^{SV} = 0.1049$ Hz and $n_1^{ST} = 0.2987$ Hz, are considered, and other parameters can be referenced from Section 4. The original modes of the deck do not meet a modal coupling problem. When motion-induced forces are engaged, the overall damping and stiffness matrices become asymmetric due to the aerodynamic effect, as reported in Eq. (16). Figure A shows the normalized PSDs of the vertical and torsional displacements at the mid span with motion-induced forces considered or not considered.

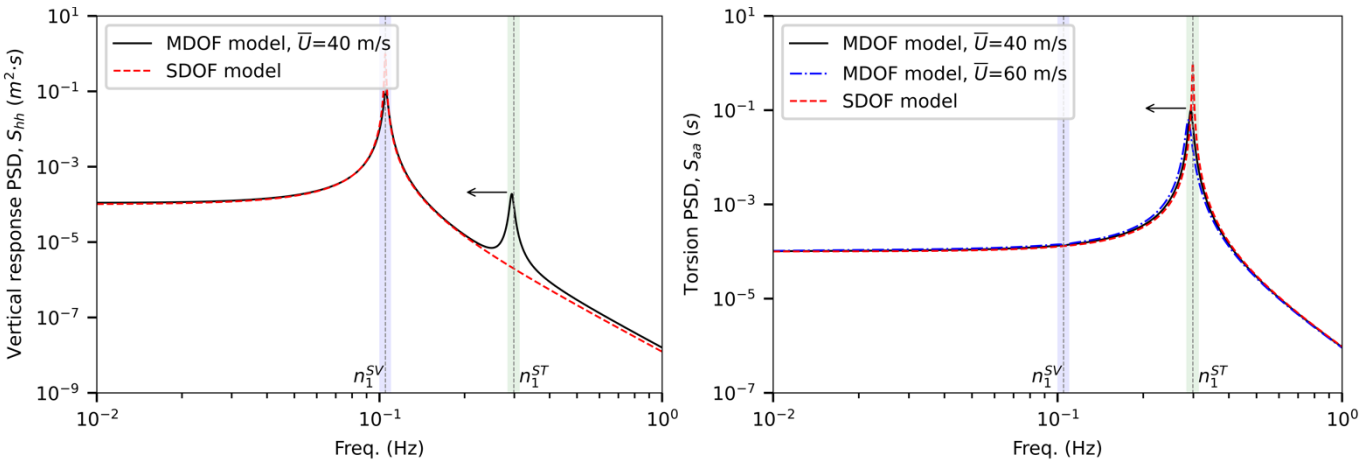

(a) Vertical response (b) Torsional response

Fig. A1. Normalized response PSDs of a two-DOF deck under stationary white-noise turbulence with motion-induced forces considered or not considered and a mean wind speed of 40 m/s.

As expected, when disregarding motion-induced forces (the SDOF model), the response PSD of a certain mode presents only one peak at its modal frequency. However, when motion-induced forces are considered, the vertical response PSD, which is supposed to have only one peak, shows an additional peak at the torsional frequency. Figure A1 (b) shows that the dominant frequency in the torsional response PSD slightly shifts to the left as the wind speed increases with respect to the non-motion-induced force case.

Appendix B

To further consolidate the effectiveness of the proposed method in simulating multimode nonstationary vibrations, the nonstationary vibrations of a two-mode model bridge subjected to synthetic nonstationary wind are simulated, and the results are compared with those of Monte Carlo method (MCM) simulations. The parameters of the model bridge are referenced from Section 4, and only the first symmetric vertical mode and the first symmetric torsional mode are considered. The nonstationary wind field consists of an analytical time-varying mean wind speed model, which is illustrated in Figure B1 (a) and can be referenced from [45], and a stationary vertical turbulence, of which the PSD is shown in Figure B1 (b). The vertical turbulence intensity of $I_w = \sigma_w/\bar{U}_{\max} = 15\%$ is considered, and turbulence in the longitudinal direction is disregarded.

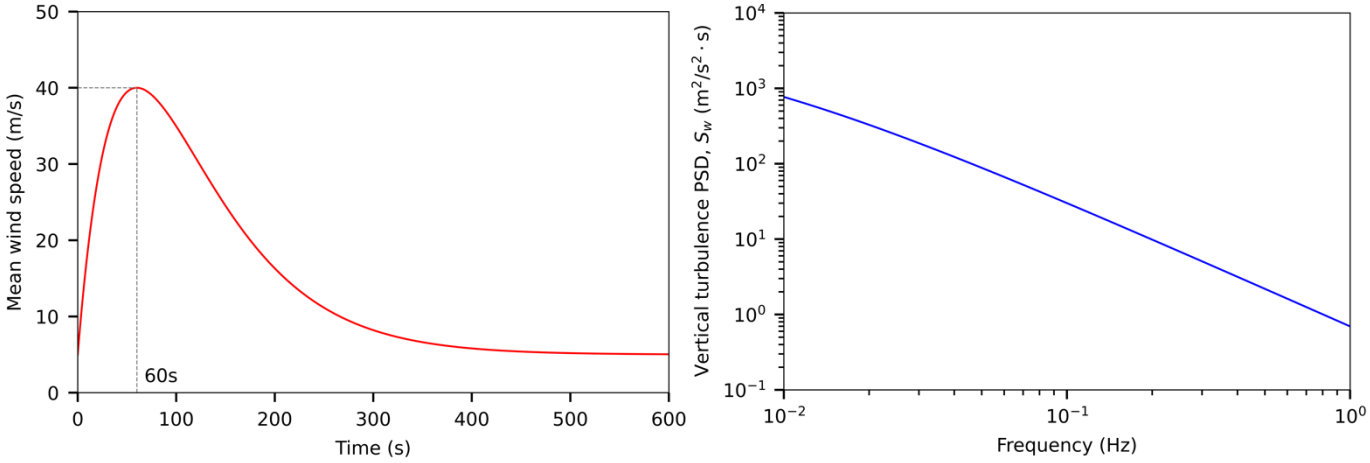

(a) Mean wind speed (b) PSD of vertical turbulence

Fig. B1. Synthetic nonstationary wind speed model.

By following the same procedures of calibrating parameters, as described in the previous sections, the state augmentation method (SAM) is then applied to calculate the instantaneous RMS responses of the vertical and rotational displacements at the mid span, as shown in Figure B2. The MCM simulation results are estimated using over 20000 samples. Only comparisons between 0~600 s are presented.

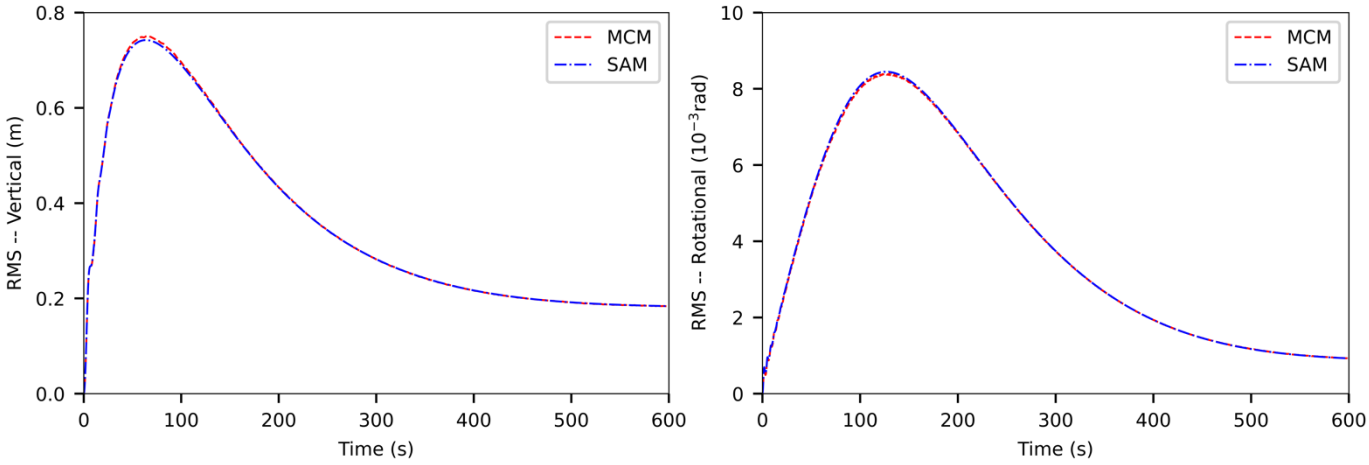

(a) Vertical displacement (b) Rotational displacement

Fig. B2. Time-varying RMSs of the mid-span displacements of a two-mode model bridge under synthetic nonstationary winds.

As shown in Figure B2, the results from the SAM and the MCM agree very well, further demonstrating the effectiveness of the proposed method in simulating multimode nonstationary vibrations. Note that the calculation time to run the SAM is approximately 3.1 s, which is quite similar to that in Section 4.1; this results incidentally justify the stable efficiency across different wind fields. However, the MCM required approximately 11 hours to obtain the statistics and was largely consumed in generating numerous excitation samples all over the frequency points and evaluating time-varying statistics all over the time instants.

References

[1] Benfratello S, Muscolino G. Filter approach to the stochastic analysis of MDOF wind-excited structures. Probabilistic engineering mechanics. 1999;14:311-21.

[2] Lei S, Ge Y, Li Q, Thompson DJ. Wave interference in railway track due to multiple wheels. Journal of Sound and Vibration. 2022;520:116620.

[3] Davenport AG. Gust loading factors. Journal of the Structural Division. 1967;93:11-34.

[4] Isyumov N. Alan G. Davenport's mark on wind engineering. Journal of Wind Engineering and Industrial Aerodynamics. 2012;104:12-24.

[5] Lombaert G, Conte JP. Random vibration analysis of dynamic vehicle-bridge interaction due to road unevenness. Journal of Engineering Mechanics. 2012;138:816-25.

[6] Huang G, Zheng H, Xu Y-l, Li Y. Spectrum models for nonstationary extreme winds. Journal of Structural Engineering. 2015;141:04015010.

[7] Zhao L, Cui W, Ge Y. Measurement, modeling and simulation of wind turbulence in typhoon outer region. Journal of Wind Engineering and Industrial Aerodynamics. 2019;195:104021.

[8] Coifman RR. Wavelet analysis and signal processing. Signal processing Part I: signal processing theory1990. p. 59-68.

[9] Huang NE, Shen Z, Long SR, Wu MC, Shih HH, Zheng Q et al. The empirical mode decomposition and the Hilbert spectrum for nonlinear and non-stationary time series analysis. Proceedings of the Royal Society of London Series A: mathematical, physical and engineering sciences. 1998;454:903-95.

[10] Kareem A. The changing dynamics of aerodynamics: New frontiers. Proceedings of the 7th Asia-Pacific Conference on Wind Engineering (APCWQ-VII), Taiwan, China2009. p. 8-12.
[11] Jain A, Jones NP, Scanlan RH. Coupled flutter and buffeting analysis of long-span bridges. Journal of Structural Engineering. 1996;122:716-25.
[12] Diana G, Stoyanoff S, Aas-Jakobsen K, Allsop A, Andersen M, Argentini T et al. IABSE Task Group 3.1 benchmark results. Part 1: Numerical analysis of a two-degree-of-freedom bridge deck section based on analytical aerodynamics. Structural Engineering International. 2020;30:401-10.
[13] Chen X, Matsumoto M, Kareem A. Aerodynamic coupling effects on flutter and buffeting of bridges. Journal of Engineering Mechanics. 2000;126:17-26.
[14] Brusco S, Solari G. Transient aeroelasticity of structures subjected to thunderstorm outflows. Engineering Structures. 2021;245:112801.
[15] Hu L, Xu Y-L, Huang W-F. Typhoon-induced non-stationary buffeting response of long-span bridges in complex terrain. Engineering Structures. 2013;57:406-15.
[16] Zadeh LA. The determination of the impulsive response of variable networks. Journal of Applied Physics. 1950;21:642-5.
[17] Kareem A, Hu L, Guo Y, Kwon D-K. Generalized wind loading chain: Time-frequency modeling framework for nonstationary wind effects on structures. Journal of Structural Engineering. 2019;145:04019092.
[18] Huang G, Chen X, Liao H, Li M. Predicting of tall building response to non-stationary winds using multiple wind speed samples. Wind & structures. 2013;17:227-44.
[19] Priestley MB. Evolutionary spectra and non‐stationary processes. Journal of the Royal Statistical Society: Series B (Methodological). 1965;27:204-29.
[20] Priestley M. Power spectral analysis of non-stationary random processes. Journal of Sound and Vibration. 1967;6:86-97.
[21] Denoël V, Carassale L. Response of an oscillator to a random quadratic velocity-feedback loading. Journal of Wind Engineering and Industrial Aerodynamics. 2015;147:330-44.
[22] Chen X. Analysis of alongwind tall building response to transient nonstationary winds. Journal of structural engineering. 2008;134:782-91.
[23] Chen X. Analysis of multimode coupled buffeting response of long-span bridges to nonstationary winds with force parameters from stationary wind. Journal of Structural Engineering. 2015;141:04014131.
[24] Guo Y, Kareem A. Non-stationary frequency domain system identification using time–frequency representations. Mechanical Systems and Signal Processing. 2016;72:712-26.
[25] Tao T, Xu Y-L, Huang Z, Zhan S, Wang H. Buffeting analysis of long-span bridges under typhoon winds with time-varying spectra and coherences. Journal of Structural Engineering. 2020;146:04020255.
[26] Lin J, Zhang W, Williams F. Pseudo-excitation algorithm for nonstationary random seismic responses. Engineering Structures. 1994;16:270-6.
[27] Hu L, Xu Y-L, Zhu Q, Guo A, Kareem A. Tropical storm–induced buffeting response of long-span bridges: Enhanced nonstationary buffeting force model. Journal of Structural Engineering. 2017;143:04017027.
[28] Lu F, Lin J, Kennedy D, Williams FW. An algorithm to study non-stationary random vibrations of

vehicle–bridge systems. Computers & Structures. 2009;87:177-85.
[29] Zhang Z, Lin J, Zhang Y, Zhao Y, Howson WP, Williams FW. Non-stationary random vibration analysis for train–bridge systems subjected to horizontal earthquakes. Engineering Structures. 2010;32:3571-82.
[30] Grigoriu M, Ariaratnam S. Response of linear systems to polynomials of Gaussian processes. 1988.
[31] Grigoriu M, Field Jr R. A method for analysis of linear dynamic systems driven by stationary non-Gaussian noise with applications to turbulence-induced random vibration. Applied Mathematical Modelling. 2014;38:336-54.
[32] Grigoriu M. Stochastic Calculus: Applications in Science and Engineering. Springer Science & Business Media; 2013.
[33] Karlin S, Taylor HE. A second course in stochastic processes: Elsevier; 1981.
[34] Itô K. 109. stochastic integral. Proceedings of the Imperial Academy. 1944;20:519-24.
[35] Risken H, Risken H. Fokker-planck equation: Springer; 1996.
[36] Alotta G, Bucher C, Di Matteo A, Di Paola M, Pirrotta A. The moment equation closure method revisited through the use of complex fractional moments. 2015.
[37] Di Paola M. Fokker Planck equation solved in terms of complex fractional moments. Probabilistic Engineering Mechanics. 2014;38:70-6.
[38] Benfratello S, Falsone G, Muscolino G. Influence of the quadratic term in the alongwind stochastic response of SDOF structures. Engineering Structures. 1996;18:685-95.
[39] Gullo I, Muscolino G, Vasta M. Non-Gaussian probability density function of SDOF linear structures under wind actions. Journal of Wind Engineering and Industrial Aerodynamics. 1998;74:1123-34.
[40] Sun J-Q, Hsu C. Cumulant-neglect closure method for nonlinear systems under random excitations. 1987.
[41] Wojtkiewicz S, Spencer Jr B, Bergman L. On the cumulant-neglect closure method in stochastic dynamics. International journal of non-linear mechanics. 1996;31:657-84.
[42] Cui W, Zhao L, Ge Y. Non-Gaussian turbulence induced buffeting responses of long-span bridges based on state augmentation method. Engineering Structures. 2022;254:113774.
[43] Soong TT, Grigoriu M. Random vibration of mechanical and structural systems. NASA STI/Recon Technical Report A. 1993;93:14690.
[44] Di Paola M, Pirrotta A. Fokker–Planck equation of the fractional Brownian motion. International Journal of Non-Linear Mechanics. 2022;147:104224.
[45] Lei S, Cui W, Patruno L, de Miranda S, Zhao L, Ge Y. Improved state augmentation method for buffeting analysis of structures subjected to non-stationary wind. Probabilistic Engineering Mechanics. 2022;69:103309.
[46] Barni N, Øiseth OA, Mannini C. Buffeting response of a suspension bridge based on the 2D rational function approximation model for self-excited forces. Engineering Structures. 2022;261:114267.
[47] Barni N, Øiseth O, Mannini C. Time-variant self-excited force model based on 2D rational function approximation. Journal of Wind Engineering and Industrial Aerodynamics. 2021;211:104523.
[48] Scanlan RH. Problematics in formulation of wind-force models for bridge decks. Journal of engineering mechanics. 1993;119:1353-75.
[49] Theodorsen T. General theory of aerodynamic instability and the mechanism of flutter. 1949.
[50] Chen X, Kareem A. Nonlinear response analysis of long-span bridges under turbulent winds. Journal of

Wind Engineering and Industrial Aerodynamics. 2001;89:1335-50.
[51] Diana G, Resta F, Rocchi D. A new numerical approach to reproduce bridge aerodynamic non-linearities in time domain. Journal of Wind Engineering and Industrial Aerodynamics. 2008;96:1871-84.
[52] Diana G, Omarini S. A non-linear method to compute the buffeting response of a bridge validation of the model through wind tunnel tests. Journal of Wind Engineering and Industrial Aerodynamics. 2020;201:104163.
[53] Diana G, Rocchi D, Argentini T, Muggiasca S. Aerodynamic instability of a bridge deck section model: Linear and nonlinear approach to force modeling. Journal of Wind Engineering and Industrial Aerodynamics. 2010;98:363-74.
[54] Page CH. Instantaneous power spectra. Journal of Applied Physics. 1952;23:103-6.
[55] Wickerhauser M. 2] RR Coifman, Y. Meyer, and MV Wickerhauser, Wavelet analysis and signal processing, Wavelets and Their Applications, ed. Ruskai et al., ISBN 0-86720-225-4, Jones and Bartlett, Boston, 1992, pp. 153 178. IEEE Transactions on Information Theory. 1992;32:712-8.
[56] Lyapunov AM. The general problem of motion stability. Annals of Mathematics Studies. 1892;17.
[57] Feller W. An introduction to probability theory and its applications, Volume 2: John Wiley & Sons; 1991.
[58] Meurer A, Smith CP, Paprocki M, Čertík O, Kirpichev SB, Rocklin M et al. SymPy: symbolic computing in Python. PeerJ Computer Science. 2017;3:e103.
[59] Chen X, Matsumoto M, Kareem A. Time domain flutter and buffeting response analysis of bridges. Journal of Engineering Mechanics. 2000;126:7-16.
[60] Xu S, Fang G, Zhao L, Ge Y, Zhang J. Aerodynamic and aerostatic performance of a long-span bridge with wide single box girder installed with vertical and horizontal stabilizers. Journal of Structural Engineering. 2023;149:04023106.
[61] Lei S, Patruno L, Mannini C, de Miranda S, Ge Y. Time-domain state-space model formulation of motion-induced aerodynamic forces on bridge decks. Journal of Wind Engineering and Industrial Aerodynamics. 2024;255:105937.
[62] Jones NP, Scanlan RH. Theory and full-bridge modeling of wind response of cable-supported bridges. Journal of Bridge Engineering. 2001;6:365-75.
[63] Lin Z, Qi W, Shenyou S, Weile C, Mingyuan W, Haili L et al. Investigation of Wind-resistance Performance of Lingdingyang Bridge with Main-span 1666 m in Shen-Zhong Link. China Journal of Highway and Transport. 2019;32:57-66.
[64] Liu P, Zhao L, Fang G, Ge Y. Explicit polynomial regression models of wind characteristics and structural effects on a long‐span bridge utilizing onsite monitoring data. Structural Control and Health Monitoring. 2021;28:e2705.
[65] Zhang L, Cui W, Zhao L, Ge Y. State augmentation method for buffeting responses of wind-sensitive structures in wind environments with large turbulence intensity. Journal of Wind Engineering and Industrial Aerodynamics. 2023;240:105498.
[66] Nadaraya EA. On estimating regression. Theory of Probability & Its Applications. 1964;9:141-2.
[67] Olesen H, Larsen SE, Højstrup J. Modelling velocity spectra in the lower part of the planetary boundary layer. Boundary-Layer Meteorology. 1984;29:285-312.